Journal of the Mechanics and Physics of Solids 59 (2011) 2082–2102

Contents lists available at ScienceDirect

Journal of the Mechanics and Physics of Solids

journal homepage: www.elsevier.com/locate/jmps

A phase-field model for incoherent martensitic transformations including plastic accommodation processes in the austenite

J. Kundin [a,*], D. Raabe [b], H. Emmerich [a]

[a] Material and Process Simulation (MPS), University Bayreuth, 95448 Bayreuth, Germany
[b] Microstructure Physics and Metal Forming, Max-Planck-Institut für Eisenforschung, 40237 Düsseldorf, Germany

ARTICLE INFO

Article history:
Received 20 December 2010
Received in revised form
7 July 2011
Accepted 10 July 2011
Available online 22 July 2011

Keywords:
Martensitic transformation
Phase field modeling
Plastic accommodation

ABSTRACT

If alloys undergo an incoherent martensitic transformation, then plastic accommodation and relaxation accompany the transformation. To capture these mechanisms we develop an improved 3D microelastic–plastic phase-field model. It is based on the classical concepts of phase-field modeling of microelastic problems (Chen, L.Q., Wang Y., Khachaturyan, A.G., 1992. Philos. Mag. Lett. 65, 15–23). In addition to these it takes into account the incoherent formation of accommodation dislocations in the austenitic matrix, as well as their inheritance into the martensitic plates based on the crystallography of the martensitic transformation. We apply this new phase-field approach to the butterfly-type martensitic transformation in a Fe–30 wt%Ni alloy in direct comparison to recent experimental data (Sato, H., Zaefferer, S., 2009. Acta Mater. 57, 1931–1937). It is shown that the therein proposed mechanisms of plastic accommodation during the transformation can indeed explain the experimentally observed morphology of the martensitic plates as well as the orientation between martensitic plates and the austenitic matrix. The developed phase-field model constitutes a general simulations approach for different kinds of phase transformation phenomena that inherently include dislocation based accommodation processes. The approach does not only predict the final equilibrium topology, misfit, size, crystallography, and aspect ratio of martensite–austenite ensembles resulting from a transformation, but it also resolves the associated dislocation dynamics and the distribution, and the size of the crystals itself.

1. Introduction

Martensitic transformation (MT) is a first-order phase transition in solid materials where a parent phase transforms diffusionless at high undercooling rates into a martensitic phase. As solid–solid MT is accompanied by elastic or elastic–plastic misfit deformations that influence the transformation kinetics and the final form of the microstructure. The different types of martensite, their orientation variants and the spatial crystal-orientation relationship (OR) within a parent austenitic phase mainly depend on the material's composition. It also defines their formation temperature and the eigenstrain tensor of the martensitic phase. A martensitic transformation might be coherent or incoherent. In the first case it is a fully reversible transformation absent of any interface dislocations.

An example of the second case, i.e. of an incoherent MT, is the butterfly-type MT in Fe–30 wt%Ni alloys. The local orientation relationships and orientation distributions between the butterfly-type α' martensitic phase and the γ austenitic

* Corresponding author.
E-mail address: julia.kundin@uni-bayreuth.de (J. Kundin).

0022-5096/$ - see front matter © 2011 Elsevier Ltd. All rights reserved.
doi:10.1016/j.jmps.2011.07.001

matrix in a Fe–30 wt%Ni alloy were recently investigated by means of electron backscanner diffraction in Sato and Zaefferer (2009) and Calcagnotto et al. (2010). Based on these experimental observations possible stages of the overall formation process were identified, which are shown in Fig. 1. According to these experimental observations, first a thin α' martensitic plate forms at relatively high temperature accommodated by multiple dislocation slip in the austenitic matrix. A habit plane close to $\{2\,2\,5\}_\gamma$ is observed on the outer side with a Kurdjumov–Sachs (K–S) OR ($\{1\,1\,1\}_\gamma \| \{0\,1\,1\}_{\alpha'}$, $\langle \bar{1}\,0\,1\rangle_\gamma \| \langle \bar{1}\,\bar{1}\,1\rangle_{\alpha'}$). In a second step, due to continued quenching, the dislocation accommodation process changes to a single or a double slip process. At this stage the habit plane close to $\{2\,5\,9\}_\gamma$ is formed on the inner interface of the martensitic plate.

The precise formation mechanisms behind the experimental observations and their physical background have not been fully elucidated so far. The assumption that the processes of elastic–plastic accommodation and relaxation processes accompanying the $\{2\,2\,5\}_F$ transformation are essential factors influencing the morphology and crystallography of the martensitic plates is commonly known in the literature (Kajiwara, 1981, 1984; Yang et al., 1984; Sandvik and Wayman, 1983). More precisely, the relaxation of the transformation strain by accommodating slip is regarded as the critical factor for $\{2\,2\,5\}_F$ plate formation. A detailed and quantitative understanding of the interaction of the mentioned mechanisms depending on the investigated material system and processing conditions is however still absent.

In this paper we intend to contribute to a better understanding of the underlying mechanisms, in particular the influence of plastic deformation on the growth kinetics of martensitic plates, via phase-field simulations. We introduce an improved 3D microelastic–plastic phase-field model, which takes into account the formation of accommodation dislocations in the austenitic matrix, as well as their inheritance into the martensitic plates based on the crystallography of the MT. The model applies the general concept of phase-field modeling of microelastic problems as it was initiated by the work of Chen et al. (1992), as well as by Wang and Khachaturyan (1997).

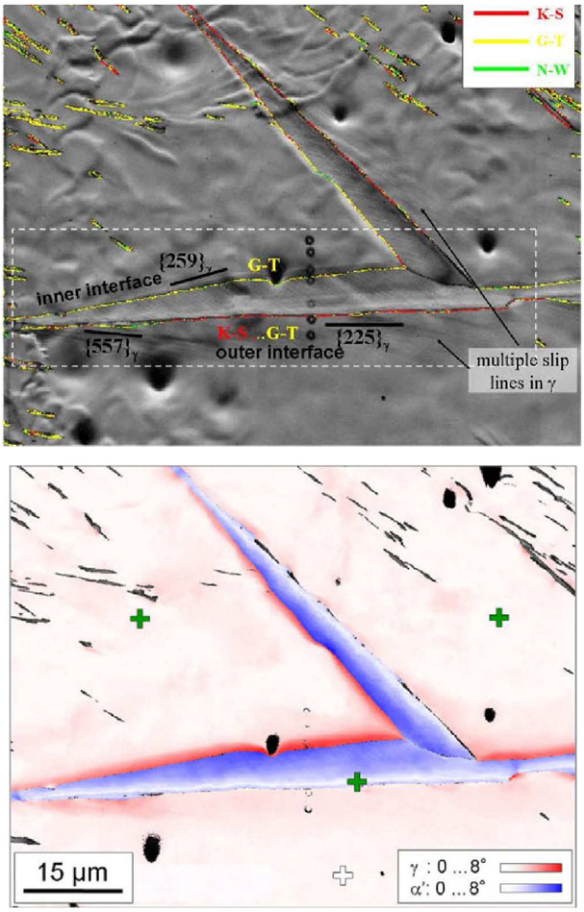

Fig. 1. Experimental microstructure of a butterfly-type martensite in the austenite matrix in Fe–30 wt%Ni alloy. Orientation relationships are shown on the top figure. The orientation gradients are shown in the bottom figure. The gradients are calculated with respect to the white crosses in the image (martensite: white…blue = 0…8°, austenite: white…red = 0…8°). (For interpretation of the references to color in this figure legend, the reader is referred to the web version of this article.)

1.1. State of the art in phase-field modeling of microelastic problems

In the past 20 years an efficient method for the simulation of the martensitic microstructure formation was developed based on the seminal works of Chen et al. (1992) and Wang and Khachaturyan (1997). This approach integrates microelasticity into the phase-field theory and is based on the fast Fourier transformation (FFT) formalism. The method which is referred to the microelasticity phase-field model (PFM) has been used to investigate martensitic transformations in single crystals (Artemev et al., 2001) and polycrystalline systems (Artemev et al., 2002), and the effect of applied stresses on the MT. These studies concern coherent transformations and do not include plastic effects due to the formation of accommodation dislocations in the austenitic matrix, which cause irreversible plastic changes in the solid phases. So that the original model deals with microelasticity but not with elastic–plastic relaxation.

Phase-field models describing dislocation kinetics were defined successively in a number of works (Koslowski et al., 2002; Ortiz and Stainier, 1999; Wang et al., 2001; Hu and Chen, 2001; Shen and Wang, 2003, 2004). In this context Wang et al. (2001) discussed the possibility of a combination of the microelasticity PFM with a PFM for dislocations. Our own earlier contribution to the field (Kundin et al., 2010) was concerned with modeling non-coherent martensitic transformations of lath-type martensites, where the dislocations were pinned to the interface between austenite and martensitic lath and their energetic contribution affected the major characteristics of the final microstructure. Due to this the introduction of a field type description of dislocation dynamics was not required.

In the current approach we go a step further to take into account that in the case of the butterfly-type martensitic transformation the accommodation dislocations can no longer be considered to be pinned to the austenite–martensite interface. Therefore, in order to achieve a versatile description of their dynamics, we employ a constitutive model for a dislocation density field (Roters et al., 2000, 2010; Ma and Roters, 2004), in which the evolution of plastic slip is described by means of an elastic driving force. Jointly with a description for the strain field of the accommodation dislocations the introduction of such a dislocation density field allows us to simulate the influence of accommodation dislocations on the transformation process. This implies also that other than Wang et al. (2001) we do not need to resolve phase-field kinetic equations for individual dislocations.

The use of a dislocation density field in our model inherits features of earlier models for the simulation of transformation induced plasticity (Tjahjanto et al., 2008). Furthermore using the phase-field microelasticity model to simulate the MT allows us to resolve the dynamics of individual martensitic plates, which cannot be done by models of the type described in Tjahjanto et al. (2008). Recently the number of works have appeared which couple the phase-field simulation with plasticity framework at mesoscale (Gaubert et al., 2010; Takaki and Tomita, 2010; Zhou et al., 2010; Yamanaka et al., 2009).

A further important feature of our model is the decomposition of the overall elastic energy in bulk and edge parts. This allows us to simulate the anisotropy of a martensitic plate correctly. In general the model can be applied to various solid–solid transformation scenarios, by adapting the input parameters according to the physics of the underlying material systems as described in Sections 2–4.

1.2. Structure and aim of this paper

The overall aim of this paper is to present a new phase-field model approach for solid–solid transformations involving dislocation dynamics. Moreover we show on the example of the butterfly-type martensitic transformation in a Fe–30 wt%Ni alloy how this model can be employed to elucidate the precise accommodation processes associated with the transformation.

The overall model consists of dynamic equations for the phase-field variables, that capture the different possible martensitic variants, as well as dynamic equations for the dislocation density fields. These are formulated based on the elastic energy contributions corresponding to the various possible crystallographic variants of the transformations. The paper is organized as follows: In Section 2 we describe the formulation of the elastic problem with accommodation dislocations, where the total elastic energy of the systems including dislocations is calculated based on the crystallography of the MT that is addressed in this paper. In particular the influence of the elastic energy on the anisotropy is discussed. Based on this we formulate the phase-field model equations for the transformation with accommodation processes in Section 3. Section 4 presents the simulation results applied to the Fe–30 wt%Ni system, as well as a comparison to experimental data. These results are critically discussed in Section 5 jointly with an outlook.

2. The solution of the elastic problem with accommodation dislocations

This section is dedicated to a derivation of the elastic energy contributions that can occur with the transformation. First we introduce the eigenstrain of a martensitic plate, which can be derived from the crystallography of the MT. Then we describe the eigenstrain of the accommodation dislocations. Both constitute the elastic part of the systems' energy and thus influence the driving force for the MT. Finally, in Section 2.4, we show how the total elastic energy can be decomposed into bulk and edge parts, where the latter one is responsible for the aspect ratio of the plates. This decomposition allows us to simulate the anisotropy of a martensitic plate directly using the formalism of the PFM.

2.1. The eigenstrain of martensitic transformation

Our starting point to determine the eigenstrain of a martensitic plate is the Bowels–Mackenzie method of analysis of MT. This method gives us the habit plane and the corresponding shape deformation in the MT.

According to Wayman (1964) in a Fe–31 wt%Ni alloy the Bain strain is given by the eigenvectors $\eta_1=\eta_2=1.136071$ and $\eta_3=0.803324$. This stain combined with the plane and the direction of the lattice invariant shear ($(1\,0\,1)_\gamma$ and $[1\,0\,\overline{1}]_\gamma$ respectively) defines the normal to the habit plane

$$\mathbf{n}_0=(0.197162,0.796841,0.571115), \tag{1}$$

the unit vector in the direction of the shape deformation

$$\mathbf{d}=(-0.223961,0.727229,-0.648829). \tag{2}$$

and the magnitude of the deformation $\varepsilon_0=0.2365$. The last value defines the displacement vector $\varepsilon_0\mathbf{d}$. The vectors $\mathbf{n}_0$ and $\mathbf{d}$ are specific for each crystallographic variant of the MT. We label a specific variant of the MT as p and consider the particular variant in Eqs. (1) and (2) as $p=1$.

For the Fe–31 wt%Ni alloy the experimental habit planes are closest to the plane with the normal $\{2\,5\,9\}_F$. The experimental and theoretical habit planes and orientation relationships determined by Breedis and Wayman (1962) are in a good agreement and apply best for the case where the dilatation parameter of the predicted habit plane is equal to 1.00137. According to the slip-type analysis in one case the martensite consists of a slipped crystal with one orientation relationship, in the other case the martensite consists of two twin-related regions, twinned with respect to a $(1\,1\,2)_B$ plane. Twinning is usually the more favorable mode of deformation at low temperature and high strain rates.

We can define the eigenstrain matrix of the MT as $\varepsilon^0_{ij}(p)=\varepsilon_0\mathbf{n}_0\otimes\mathbf{d}$ from the estimated habit plane and the direction of the shape deformation (Bhadeshia, 2001)

$$\varepsilon^0_{ij}(p=1)=\begin{pmatrix}-0.0098 & -0.0399 & -0.0286\\ 0.0320 & 0.1294 & 0.0928\\ -0.0286 & -0.1155 & -0.0838\end{pmatrix}. \tag{3}$$

Here $\mathbf{n}_0\otimes\mathbf{d}$ is the tensor product of the vectors.

2.2. Modeling the dislocation elastic contributions

In order to formulate the micro-mechanical contributions of the accommodation dislocations in the total energy functional underlying our phase-field model formulation we describe in this section the strain of accommodation dislocations. This strain arises during the MT and corresponds to a plastic deformation in the γ austenitic phase, which is then inherited in the α' phase resulting in orientation gradients.

Further we consider a dislocation with Burgers vector $\mathbf{b}^{(\alpha)}$ (with unit m) and slip plane with normal $\mathbf{n}^{(\alpha)}$ (without a unit) in a Cartesian coordinate system defined by the cubic lattice of the parent austenitic phase, where α is an index corresponding to a slip system. The illustration of an edge dislocation with all constitutive vectors is presented in Fig. 2. Let components of a displacement vector created by a dislocation be given by

$$u^d_i(\alpha,\mathbf{r},\mathbf{r}_0)=b^{(\alpha)}_i\mathrm{H}_a(\mathbf{n}^{(\alpha)}\Delta\mathbf{r})\mathrm{H}(-\mathbf{e}^{(\alpha)}\Delta\mathbf{r}), \tag{4}$$

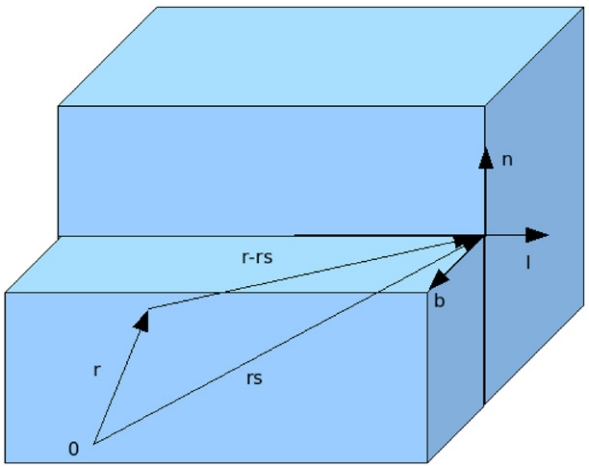

Fig. 2. Schematic illustration of an edge dislocation. Here, b is the Burgers vector, and n is the unit vector normal to the slip plane.

where $H(x)$ is the Heaviside step function, $H_a(x)=1$ if $0\le x<a$ and 0 otherwise, a is the lattice constant and represents the dislocation core size, $\Delta\mathbf{r}=\mathbf{r}-\mathbf{r}_0$ with a site $\mathbf{r}_0$ located on the dislocation line, $\mathbf{n}^{(\alpha)}\Delta\mathbf{r}$ is a scalar product and $\mathbf{e}^{(\alpha)}=[\mathbf{n}^{(\alpha)}\times\mathbf{l}(\mathbf{r}_0)^{(\alpha)}]$ is a vector product of the normal $\mathbf{n}^{(\alpha)}$ and the tangential unit vector to a dislocation line $\mathbf{l}^{(\alpha)}$ on a site $\mathbf{r}_0$.

The displacement vector $\mathbf{u}^d(\alpha,\mathbf{r},\mathbf{r}_0)$ with components $u_i^d(\alpha,\mathbf{r},\mathbf{r}_0)=b_i^{(\alpha)}$ is defined on a volume $\Omega:\ 0\le\mathbf{n}^{(\alpha)}\Delta\mathbf{r}<a$ and $\mathbf{e}^{(\alpha)}\Delta\mathbf{r}<0$). At $a\to0$ the displacement is defined on the half plane $\mathbf{n}^{(\alpha)}\Delta\mathbf{r}=0$, $\mathbf{e}^{(\alpha)}\Delta\mathbf{r}<0$ with the normal $\mathbf{n}^{(\alpha)}$.

Let the unit vector in the direction of the Burgers vector be defined as $\mathbf{m}^{(\alpha)}=\mathbf{b}^{(\alpha)}/b^{(\alpha)}$. This vector expresses the slip direction of a dislocation. For an edge dislocation $\mathbf{m}^{(\alpha)}=\mathbf{e}^{(\alpha)}$ and for a screw dislocation $\mathbf{m}^{(\alpha)}=\mathbf{l}^{(\alpha)}$.

From linear elasticity the eigenstrain tensor of a dislocation can be given by

$$\varepsilon_{ij}^d=\frac{1}{2}\left(\frac{\partial u_i^d}{\partial r_j}+\frac{\partial u_j^d}{\partial r_i}\right). \tag{5}$$

By substituting (4) in (5) we get

$$\varepsilon_{ij}^d(\alpha,\mathbf{r},\mathbf{r}_0)=\tfrac{1}{2}(b_i^{(\alpha)}n_j^{(\alpha)}+b_j^{(\alpha)}n_i^{(\alpha)})\delta(\mathbf{n}^{(\alpha)}\Delta\mathbf{r})\mathrm{H}(-\mathbf{e}^{(\alpha)}\Delta\mathbf{r})-\tfrac{1}{2}(b_i^{(\alpha)}e_j^{(\alpha)}+b_j^{(\alpha)}e_i^{(\alpha)})\delta(\mathbf{e}^{(\alpha)}\Delta\mathbf{r})\mathrm{H}_a(\mathbf{n}^{(\alpha)}\Delta\mathbf{r}), \tag{6}$$

where $\delta(x)$ is the Dirac delta function. The second term in Eq. (7) represents the strain of the dislocation core.

For the convenience we introduce the symmetric Schmid tensor for the slip system α, $\hat{\mathbf{M}}^{(\alpha)}$, with the components

$$\mathrm{M}_{ij}^{(\alpha)}=\tfrac{1}{2}(m_i^{(\alpha)}n_j^{(\alpha)}+m_j^{(\alpha)}n_i^{(\alpha)}), \tag{7}$$

and the symmetric tensor $\hat{\mathbf{Q}}^{(\alpha)}$

$$\mathrm{Q}_{ij}^{(\alpha)}=\tfrac{1}{2}(m_i^{(\alpha)}e_j^{(\alpha)}+m_j^{(\alpha)}e_i^{(\alpha)}). \tag{8}$$

Consider a distribution of dislocations with a density $\rho_d^{(\alpha)}$, which is the value of the total dislocation line length per unit volume. Consider a cubic box with a size L. The volume corresponding to one dislocation in this box is equal to $V_d=(1/\sqrt{\rho_d})^2L$. For the eigenstrain tensor of the dislocation distribution we calculate an averaged value over the volume V_d

$$\varepsilon_{ij}^d(\alpha,\mathbf{r})=b^{(\alpha)}\mathrm{M}_{ij}^{(\alpha)}\frac{1}{V_d}\int_0^{V_d}\delta(\mathbf{n}^{(\alpha)}(\mathbf{r}-\mathbf{r}'))\mathrm{H}(-\mathbf{e}^{(\alpha)}(\mathbf{r}-\mathbf{r}'))\,\mathrm{d}\mathbf{r}'+b^{(\alpha)}\mathrm{Q}_{ij}^{(\alpha)}\frac{1}{V_d}\int_0^{V_d}\delta(\mathbf{e}^{(\alpha)}(\mathbf{r}-\mathbf{r}'))\mathrm{H}_a(\mathbf{n}^{(\alpha)}(\mathbf{r}-\mathbf{r}'))\,\mathrm{d}\mathbf{r}'. \tag{9}$$

Here the first integral is equal to $(1/\sqrt{\rho_d})L$ and the second integral is equal to $(1/\sqrt{\rho_d})a$. We define $\phi_\alpha^d(\mathbf{r})=b^{(\alpha)}\sqrt{\rho_d^{(\alpha)}(\mathbf{r})}$ as a dimensionless dislocation function and $\phi_\alpha^{d,\mathrm{cor}}(\mathbf{r})=b^{(\alpha)}a\rho_d^{(\alpha)}(\mathbf{r})$ as a dimensionless function of the dislocation core. After the integration of Eq. (9) we get

$$\varepsilon_{ij}^d(\alpha,\mathbf{r})=\mathrm{M}_{ij}^{(\alpha)}\phi_\alpha^d(\mathbf{r})+\mathrm{Q}_{ij}^{(\alpha)}\phi_\alpha^{d,\mathrm{core}}(\mathbf{r}). \tag{10}$$

For the case $a\ll1/\sqrt{\rho_d}$ the second term representing the dislocation core can be omitted. For the calculation of the elastic energy in Section 2.3 we use only the first term, because for the second term the evaluation procedure is similar and we do not find it convenient to overburden the paper.

The calculation of the time evolution of the dislocation density based on the above assumptions is presented in Section 3.4. In our simulations we assume: (i) Transformation-induced plastic deformation is hindered in the martensite, and the evolution of plastic slip during the process occurs only in the austenitic phase. (ii) The dislocations are inherited in the martensite without change of their eigenstrain, because, according to the experimental results, the slip systems in the austenite matrix and martensite have approximately similar directions (Umemoto and Tamura, 1982; Umemoto et al., 1983; Sato and Zaefferer, 2009). (iii) The lattice rotation due to dislocation glide is not considered in the model.

2.3. The calculation of the total elastic energy

Following Wang and Khachaturyan (1997) and Artemev et al. (2002), we consider a coherent multiphase mixture with the local stress–free strain tensor $\varepsilon_{ij}^0(p,\mathbf{r})=\varepsilon_{ij}^0(p)\eta_p(\mathbf{r})$ reflecting the eigenstrain and $\eta_p(\mathbf{r})$ is the shape function of a martensitic plate of the pth crystallographic variant. The shape function reflects the phase-field variable in the PFM (see Section 4). The local stress–free plastic strain tensor caused by dislocations of an α th slip system according to Eq. (10) is given by $\varepsilon_{ij}^d(\alpha,\mathbf{r})$. Here ν is the number of the martensitic variants and μ is the number of the slip systems.

We write $\varepsilon_{ij}(\mathbf{r})$ to denote the total strain. Then Hooke's law gives the local elastic stress

$$\sigma_{ij}^{el}(\mathbf{r})=\lambda_{ijkl}\left[\varepsilon_{kl}(\mathbf{r})-\left(\sum_{p=1}^{\nu}\varepsilon_{kl}^0(p,\mathbf{r})+\sum_{\alpha=1}^{\mu}\varepsilon_{kl}^d(\alpha,\mathbf{r})\right)\right]. \tag{11}$$

Requiring mechanical equilibrium yields the following set of equations:

$$\sum_{j=1}^{3}\frac{\partial\sigma_{ij}^{el}(\mathbf{r})}{\partial r_j}=0. \tag{12}$$

Since analytic solutions of such equations can be obtained for the strain distribution of a macroscopically homogeneous but microscopically (structurally) inhomogeneous body (Khachaturyan, 1983), it is reasonable to decompose the total strain $\varepsilon_{ij}(\mathbf{r})$ as a sum of homogeneous $\overline{\varepsilon}_{ij}$ and heterogeneous $\delta\varepsilon_{ij}(\mathbf{r})$ strains,

$$\varepsilon_{ij}(\mathbf{r}) = \overline{\varepsilon}_{ij} + \delta\varepsilon_{ij}(\mathbf{r}), \tag{13}$$

such that $\int_V \delta\varepsilon_{ij}(\mathbf{r})\, d\mathbf{r} = 0$. The homogeneous strain is equal to the volume average of the sum of the composition eigenstrain and the dislocation eigenstrain (10),

$$\overline{\varepsilon}_{ij} = \overline{\varepsilon}_0 + \overline{\varepsilon}_d = \frac{1}{V}\sum_{p=1}^{v} \varepsilon_{ij}^0(p) \int_V \eta_p(\mathbf{r})\, d\mathbf{r} + \frac{1}{V}\sum_{\alpha=1}^{\mu} M_{ij}^{(\alpha)} \int_V \phi_\alpha^d(\mathbf{r})\, d\mathbf{r}, \tag{14}$$

where V is the volume of the system.

Before we proceed to the calculation of the heterogeneous displacement contribution let us define $u_k(\mathbf{r})$ as the kth component of the displacement, related to the strain via the formula

$$\delta\varepsilon_{ij} = \frac{1}{2}\left(\frac{\partial u_i}{\partial r_j} + \frac{\partial u_j}{\partial r_i}\right). \tag{15}$$

In order to find the heterogeneous displacement, one has to substitute Eqs. (11), (13) and (15) into the mechanical equilibrium equations (12) and obtains

$$\lambda_{ijkl}\frac{\partial^2 u_k(\mathbf{r})}{\partial r_j \partial r_l} = \sum_{p=1}^{v} \sigma_{ij}^0(p)\frac{\partial \Delta\eta_p(\mathbf{r})}{\partial r_j} + \sum_{\alpha=1}^{\mu} \sigma_{ij}^d(\alpha)\frac{\partial \Delta\phi_\alpha^d(\mathbf{r})}{\partial r_j} \tag{16}$$

where λ_{ijkl} are the elastic constants, $\sigma_{ij}^0(p) \coloneqq \lambda_{ijkl}\varepsilon_{kl}^0(p)$, $\sigma_{ij}^d(\alpha) \coloneqq \lambda_{ijkl}M_{kl}^\alpha$ are the elastic stresses. Furthermore $\Delta\eta_p(\mathbf{r}) = \eta_p(\mathbf{r}) - \langle \eta_p(\mathbf{r})\rangle$, $\Delta\phi_\alpha^d(\mathbf{r}) = \phi_\alpha^d(\mathbf{r}) - \langle \phi_\alpha^d(\mathbf{r})\rangle$, where $\langle\cdot\rangle$ represents the average over the entire volume.

Eq. (16) can be solved in Fourier space. One finds

$$u_k(\mathbf{k}) = -\mathrm{i}G_{ik}(\mathbf{k})\left[\sum_{p=1}^{v} \sigma_{ij}^0(p)\Delta\widehat{\eta}_p(\mathbf{k}) + \sum_{\alpha=1}^{\mu} \sigma_{ij}^d(\alpha)\Delta\widehat{\phi}_\alpha^d(\mathbf{k})\right]k_j, \tag{17}$$

where $G_{ik}(\mathbf{k})$ is the Green tensor which is inverse to $G_{ik}^{-1}(\mathbf{k}) = k^2\lambda_{ijkl}n_j n_l$, $\mathbf{n} = \mathbf{k}/k$ is a unit wave vector with the magnitude k and i denotes the imaginary unit. Furthermore $\widehat{\eta}_p(\mathbf{k})$ and $\widehat{\phi}_\alpha^d(\mathbf{k})$ denote Fourier transforms.

Successively we can obtain the heterogeneous strain in the Fourier space as

$$\delta\hat{\varepsilon}_{ij}(\mathbf{k}) = \frac{\mathrm{i}}{2}(u_i(\mathbf{k})k_j + u_j(\mathbf{k})k_i). \tag{18}$$

The total elastic energy is given by

$$E_{\mathrm{elast}}^{\mathrm{tot}} = E_0 + \frac{1}{2}\int_V \lambda_{ijkl}\varepsilon_{ij}(\mathbf{r})\varepsilon_{kl}(\mathbf{r})\, d\mathbf{r}, \tag{19}$$

where E_0 measures the difference between the stress free state and the unstrained state,

$$E_0 = \frac{V}{2}\sum_{p=1}^{v} \lambda_{ijkl}\varepsilon_{ij}^0(p)\varepsilon_{kl}^0(p)\langle \eta_p(\mathbf{r})^2\rangle + \sum_{p=1}^{v}\sum_{\alpha=1}^{\mu} \lambda_{ijkl}\varepsilon_{ij}^0(p)M_{kl}^\alpha\langle \eta_p(\mathbf{r})\phi_\alpha^d(\mathbf{r})\rangle + \frac{V}{2}\sum_{\alpha=1}^{\mu} \lambda_{ijkl}M_{ij}^\alpha M_{kl}^\alpha\langle \phi_\alpha^d(\mathbf{r})^2\rangle. \tag{20}$$

Substituting Eq. (13) into Eq. (19) and taking into account that by definition $\int_V \delta\varepsilon_{ij}(\mathbf{r})\, d\mathbf{r} = 0$, yields

$$E_{\mathrm{elast}}^{\mathrm{tot}} = E_0 - \frac{V}{2}\lambda_{ijkl}\overline{\varepsilon}_{ij}\overline{\varepsilon}_{kl} - \frac{1}{2}\int_V \lambda_{ijkl}\delta\varepsilon_{ij}(\mathbf{r})\delta\varepsilon_{kl}(\mathbf{r})\, d\mathbf{r}, \tag{21}$$

where the second term on the right side is the energy change caused by a homogeneous strain relaxation, $E_{\mathrm{relax}}^{\mathrm{homo}}$, and the third term is the energy change caused by a heterogeneous relaxation of displacements $\mathbf{u}(\mathbf{r})$, $E_{\mathrm{relax}}^{\mathrm{heter}}$ (Khachaturyan, 1983). Substituting Eqs. (14) and (18) into Eq. (21) gives the homogeneous and heterogeneous strain relaxation terms. The resulting equation for the total elastic energy becomes

$$\begin{aligned}
E_{\mathrm{elast}}^{\mathrm{tot}} = {} & \frac{1}{2}\sum_{p,q=1}^{v} \fint \frac{\mathrm{d}^3\mathbf{k}}{(2\pi)^3}[\lambda_{ijkl}\varepsilon_{ij}^0(p)\varepsilon_{kl}^0(q) - \mathbf{n}\hat{\boldsymbol{\sigma}}^0(p)\hat{\boldsymbol{\Omega}}(\mathbf{n})\hat{\boldsymbol{\sigma}}^0(q)\mathbf{n}]\widehat{\eta}_p(\mathbf{k})\widehat{\eta}_q^*(\mathbf{k}) \\
& + \frac{1}{2}\sum_{p=1}^{v}\sum_{\alpha=1}^{\mu} \fint \frac{\mathrm{d}^3\mathbf{k}}{(2\pi)^3}[\lambda_{ijkl}\varepsilon_{ij}^0(p)M_{kl}(\alpha) - \mathbf{n}\hat{\boldsymbol{\sigma}}^0(p)\hat{\boldsymbol{\Omega}}(\mathbf{n})\hat{\boldsymbol{\sigma}}^0(\alpha)\mathbf{n}]\widehat{\eta}_p(\mathbf{k})\widehat{\phi}_\alpha^{d*}(\mathbf{k}) \\
& + \frac{1}{2}\sum_{p=1}^{v}\sum_{\alpha=1}^{\mu} \fint \frac{\mathrm{d}^3\mathbf{k}}{(2\pi)^3}[\lambda_{ijkl}M_{ij}(\alpha)\varepsilon_{kl}^0(p) - \mathbf{n}\hat{\boldsymbol{\sigma}}^0(\alpha)\hat{\boldsymbol{\Omega}}(\mathbf{n})\hat{\boldsymbol{\sigma}}^0(p)\mathbf{n}]\widehat{\phi}_\alpha^d(\mathbf{k})\widehat{\eta}_p^*(\mathbf{k}) \\
& + \frac{1}{2}\sum_{\alpha,\beta=1}^{\mu} \fint \frac{\mathrm{d}^3\mathbf{k}}{(2\pi)^3}[\lambda_{ijkl}M_{ij}(\alpha)M_{kl}(\beta) - \mathbf{n}\hat{\boldsymbol{\sigma}}^0(\alpha)\hat{\boldsymbol{\Omega}}(\mathbf{n})\hat{\boldsymbol{\sigma}}^0(\beta)\mathbf{n}]\widehat{\phi}_\alpha^d(\mathbf{k})\widehat{\phi}_\beta^{d*}(\mathbf{k}),
\end{aligned} \tag{22}$$

where $\{\cdot\}^*$ denotes the complex conjugate of $\{\cdot\}$ and the symbol $\fint$ describes the integral excluding the point $\mathbf{k}=0$. The components of the inverse tensor Ω_{ij}^{-1} are defined with respect to a vector $\mathbf{n}$ as (Khachaturyan, 1983)

$$\Omega_{jk}(\mathbf{n})^{-1} = \lambda_{jilk} n_i n_l. \tag{23}$$

The functions in square brackets are in the following referred to as strain energy functions labeled as $B_{pq}(\mathbf{n})$, $B_{p\alpha}(\mathbf{n})$, $B_{\alpha p}(\mathbf{n})$ and $B_{\alpha\beta}(\mathbf{n})$.

2.4. Decomposition of the elastic energy in bulk and edge parts

To simulate the microstructure evolution for the butterfly-type martensite, which consist of two martensitic plate of two types, we consider separately the energy of the elastic interaction of a plate with itself or so-called self-energy and the energy of the interaction between two martensitic plates. This procedure allows us to simplify the simulation and evaluate the elastic part of the interface energy (Section 2.4).

Following Khachaturyan (1983) we write Eq. (22) for a single martensitic plate, which is simplified as

$$E_{\text{elast}}^{\text{self}} = \frac{1}{2}\int \frac{\mathrm{d}^3\mathbf{k}}{(2\pi)^3} B_{pp}(\mathbf{n}) |\widehat{\eta}_p(\mathbf{k})|^2. \tag{24}$$

Since in Eq. (24) $B_{pp}(\mathbf{n}) \geq 0$ and $|\widehat{\eta}_p(\mathbf{k})|^2 > 0$, one obtains

$$E_{\text{elast}}^{\text{self}} = \frac{1}{2}\int \frac{\mathrm{d}^3\mathbf{k}}{(2\pi)^3} B_{pp}(\mathbf{n}) |\widehat{\eta}_p(\mathbf{k})|^2 \geq \frac{1}{2}(\min B_{pp}(\mathbf{n})) \int \frac{\mathrm{d}^3\mathbf{k}}{(2\pi)^3} |\widehat{\eta}_p(\mathbf{k})|^2, \tag{25}$$

where $\min B_{pp}(\mathbf{n})$ is the minimum value of the function $B_{pp}(\mathbf{n})$. Let us define $B_{pp}(\mathbf{n}_0) = \min B_{pp}(\mathbf{n})$, where the unit vector $\mathbf{n}_0$ define the direction, where the function $B_{pp}(\mathbf{n})$ has its minimum. Further we define $\Delta B_{pp}(\mathbf{n}) = B_{pp}(\mathbf{n}) - B_{pp}(\mathbf{n}_0)$. Then we write the strain energy in the form

$$E_{\text{elast}}^{\text{self}} = E_{\text{bulk}}^{\text{self}} + E_{\text{edge}}^{\text{self}}, \tag{26}$$

where

$$E_{\text{bulk}}^{\text{self}} = \frac{1}{2} B_{pp}(\mathbf{n}_0) \int \frac{\mathrm{d}^3\mathbf{k}}{(2\pi)^3} |\widehat{\eta}_p(\mathbf{k})|^2 \tag{27}$$

is the bulk elastic energy and

$$E_{\text{edge}}^{\text{self}} = \frac{1}{2}\int \frac{\mathrm{d}^3\mathbf{k}}{(2\pi)^3} \Delta B_{pp}(\mathbf{n}) |\widehat{\eta}_p(\mathbf{k})|^2 \tag{28}$$

is the edge elastic energy. This term quantifies the energy that belongs to that part of the interface which deviates from the habit plane.

The precise calculation of the integral (28) for a plate-like inclusion was introduced by (Khachaturyan, 1983)

$$E_{\text{edge}}^{\text{self}} = \oint \delta(\mathbf{n}_{\text{int}})\, dl, \tag{29}$$

where

$$\delta(\mathbf{n}_{\text{int}}) \approx \left(\frac{D^2}{4\pi} \ln\frac{L}{D}\right) \beta_{ij}(\mathbf{n_0}) n_i^{\text{int}} n_j^{\text{int}}, \tag{30}$$

with D and L being a width and a length of an inclusion, respectively. Here $\mathbf{n}_{\text{int}} = [\mathbf{n_0} \times \mathbf{dl}]$ is the normal to the habit plane $\mathbf{n_0}$ and normal to the line element $\mathbf{dl}$ of the perimeter contour describing the shape of a martensitic plate in the habit plane. β_{ij} are the components of the second-rank tensor

$$\beta_{ij}(\mathbf{n}_0) = \begin{pmatrix} \frac{\partial^2 \Delta B_{pp}(\mathbf{n})}{\partial n_x^2} & \frac{\partial^2 \Delta B_{pp}(\mathbf{n})}{\partial n_x \partial n_y} \\ \frac{\partial^2 \Delta B_{pp}(\mathbf{n})}{\partial n_x \partial n_y} & \frac{\partial^2 \Delta B_{pp}(\mathbf{n})}{\partial n_y^2} \end{pmatrix}_{n\,=\,n_0}. \tag{31}$$

The eigenvalues of this tensor determine the equilibrium inclusion shape in the habit plane. The edge energy can be interpreted as the energy of a dislocation loop along the perimeter of a plate-like inclusion. Based on this we present an estimation of the equilibrium shape of a thin martensitic plate in Section 2.5.

2.5. The estimation of the equilibrium shape of a martensitic plate based on the interface elastic energy

According to Khachaturyan (1983), to calculate the shape of a plate-like inclusion in the habit plane, one first has to calculate the vector $\mathbf{n}_0$ normal to the habit plane and the unit vector in the direction of the displacement $\mathbf{d}$ for the particularly considered variant of the MT. Then one has to determine the components of the tensor $\beta_{ij}(\mathbf{n}_0)$, which is

responsible for the value of the shape dependent part of the elastic strain energy or so-called edge energy (see Eq. (29)). The components of the vector $\beta_{ij}(\mathbf{n}_0)$ are defined as

$$\beta_{ij}(\mathbf{n}_0) = \varepsilon_0^2 \Omega_{ij}^{-1}(\mathbf{d}) - (\hat{\sigma}_1 \Omega_{ij}(\mathbf{n}_0) \hat{\sigma}_1^+)_{ij}, \tag{32}$$

where the stress tensor $\hat{\boldsymbol{\sigma}}_1$ is defined as

$$(\hat{\boldsymbol{\sigma}}_1)_{ij} = \varepsilon_0 \lambda_{ilmj} d_l n_m^0. \tag{33}$$

and $\hat{\sigma}_1^+$ is the Hermitian transpose.

By using the nonzero components of the elastic stiffness tensor for a cubic crystal

$$\lambda_{1111} = \lambda_{2222} = \lambda_{3333} = c_{11},$$

$$\lambda_{1122} = \lambda_{1133} = \lambda_{2233} = c_{12},$$

$$\lambda_{1212} = \lambda_{1313} = \lambda_{2323} = c_{44},$$

$$\lambda_{1221} = \lambda_{2112} = \lambda_{1331} = c_{44}, \tag{34}$$

and the symmetry relations for the tensor λ_{ijkl} the components of the inverse tensor $\Omega_{ij}^{-1}(\mathbf{n})$ can be written in the detailed form according to Eq. (23)

$$\Omega_{ii}^{-1}(\mathbf{n}) = c_{44} + (c_{11} - c_{44}) n_i^2,$$

$$\Omega_{ij}^{-1}(\mathbf{n}) = (c_{12} + c_{44}) n_i n_j. \tag{35}$$

From the definition (33) one can obtain

$$\sigma_{11}^{(1)} = \sigma_{22}^{(1)} = c_{44}\varepsilon_0 \left[\frac{c_{11}}{c_{44}} d_1 n_1^0 + d_2 n_2^0 + d_3 n_3^0 \right],$$

$$\sigma_{33}^{(1)} = c_{44}\varepsilon_0 \left[\frac{c_{11}}{c_{44}} d_3 n_3^0 + d_1 n_1^0 + d_2 n_2^0 \right],$$

$$\sigma_{ij}^{(1)} = c_{44}\varepsilon_0 \left[\frac{c_{11}}{c_{44}} d_i n_j^0 + d_j n_i^0 \right] \quad \text{if } i \neq j, \tag{36}$$

where $\mathbf{n}_0 = (n_1^0, n_2^0, n_3^0)$ and $\mathbf{d} = (d_1, d_2, d_3)$.

Using the elastic constant values for Fe-31.5%Ni (Hausch and Warlimont, 1973)

$$c_{11} = 1.404 \times 10^{11} \text{ Pa},$$

$$c_{12} = 0.84 \times 10^{11} \text{ Pa},$$

$$c_{14} = 1.121 \times 10^{11} \text{ Pa}, \tag{37}$$

the habit plane and the slip direction from Section 2.1 (Eqs. (1) and (2)) for variant $p=1$ we find the corresponding stress tensor

$$\hat{\sigma}_1 = c_{44}\varepsilon_0 \begin{pmatrix} 0.1536 & 0.0097 & -0.2238 \\ -0.0710 & 0.3111 & -0.2058 \\ -0.2238 & 0.0279 & 0.0712 \end{pmatrix}. \tag{38}$$

For the components of the tensor $\Omega_{ij}(\mathbf{n_0})$ the substitution of values (1) and (37) into (23) and the calculation of the inverse matrix yields

$$\hat{\boldsymbol{\Omega}}(\mathbf{n_0}) = \frac{1}{c_{44}} \begin{pmatrix} 1.4326 & -0.3941 & 0.0346 \\ -0.3941 & 2.7754 & -2.3339 \\ 0.0346 & -2.3339 & 3.1214 \end{pmatrix}. \tag{39}$$

The components of the inverse tensor $\Omega_{ij}^{-1}(\mathbf{l})$ from Eq. (23) are

$$\hat{\boldsymbol{\Omega}}^{-1}(\mathbf{d}) = c_{44} \begin{pmatrix} 0.7746 & -0.2849 & 0.2542 \\ -0.2839 & 1.0154 & -0.8254 \\ 0.2542 & -0.8254 & 0.9611 \end{pmatrix}. \tag{40}$$

From Eq. (32) it can be seen that the vector $\mathbf{n}_0$ is an eigenvector ($\mathbf{e}_3$) of the matrix $\hat{\boldsymbol{\beta}}(\mathbf{n}_0)$. Then for the vectors $\mathbf{n}_0 = \langle 2\ 9\ 5 \rangle_F$ and $\mathbf{d}$ given by (1) and (2) the unit vector in the direction $\langle 2\ \overline{1}\ 1 \rangle_F$

$$\mathbf{e}_2 = (-0.8165, -0.4082, 04082) \tag{41}$$

is the second eigenvector of the matrix $\hat{\boldsymbol{\beta}}(\mathbf{n}_0)$.

By the multiplication of two eigenvectors we can identify the last eigenvector in the direction close to $\langle \overline{6}\ \overline{4}\ 9 \rangle_F$

$$\mathbf{e}_1 = (-0.5585, -0.3858, 0.7311). \tag{42}$$

With this eigenvectors the eigenvalues of the matrix $\hat{\boldsymbol{\beta}}(\mathbf{n}_0)$ can be defined by

$$\beta_1 = \varepsilon_0^2(\mathbf{e}_1\hat{\boldsymbol{\Omega}}^{-1}(\mathbf{d})\mathbf{e}_1) - (\hat{\sigma}_1\mathbf{e}_1\hat{\boldsymbol{\Omega}}^{-1}(\mathbf{n}_0)\hat{\sigma}_1^{+}\mathbf{e}_1),$$

$$\beta_2 = \varepsilon_0^2(\mathbf{e}_2\hat{\boldsymbol{\Omega}}^{-1}(\mathbf{d})\mathbf{e}_2) - (\hat{\sigma}_1\mathbf{e}_2\hat{\boldsymbol{\Omega}}^{-1}(\mathbf{n}_0)\hat{\sigma}_1^{+}\mathbf{e}_2) \tag{43}$$

as

$$\beta_1 = 1.4390 c_{44}\varepsilon_0^2,$$

$$\beta_2 = 0.6161 c_{44}\varepsilon_0^2. \tag{44}$$

It can be also shown that for the habit plane the eigenvalue is going to zero $\beta_3 = 0$.

The same procedure carried out for the habit plane $\{2\ 5\ 2\}_F$ yields the values

$$\beta_1 = 1.7046 c_{44}\varepsilon_0^2,$$

$$\beta_2 = 0.348 c_{44}\varepsilon_0^2 \tag{45}$$

with the eigenvectors

$$\mathbf{e}_1 = (0.5773, -0.5773, 0.5773),$$

$$\mathbf{e}_2 = (-0.7035, 0, 0.7035), \tag{46}$$

which correspond to the directions $\langle 1\ \overline{1}\ 1 \rangle_F$ and $\langle \overline{1}\ 0\ 1 \rangle_F$. Assume L_1 is the size of a martensitic plate in the direction $\mathbf{e}_1$ with the eigenvalue β_1 and L_2 is the size in the direction $\mathbf{e}_2$ with the eigenvalue β_2. For $\beta_1 > \beta_2$ the anisotropy parameter is defined as

$$\alpha_{12} = \frac{\beta_1 - \beta_2}{\beta_1}. \tag{47}$$

According to Khachaturyan (1983) the width-to-length ratio L_2/L_1 for a martensitic plate can be found as

$$\frac{L_2}{L_1} = \begin{cases} 1-\alpha_{12} & \text{if} \quad \alpha_{12} \le 0.5, \\ \dfrac{1}{2}\sqrt{\dfrac{1-\alpha_{12}}{\alpha_{12}}} & \text{if} \quad \alpha_{12} \ge 0.5. \end{cases} \tag{48}$$

So that for the habit plane $\{2\ 9\ 5\}_F$, $\alpha_{12} = 0.5719$ and $L_2/L_1 = 0.4281$ and for the habit plane $\{2\ 5\ 2\}_F$, $\alpha_{12} = 0.7558$ and $L_2/L_1 = 0.2532$.

The larger the parameter β_i is, the larger is also the growth rate in the direction $\mathbf{e}_i$. In the particular direction $\mathbf{e}_3$ where $\beta_3 = 0$ the growth rate is equal to zero. The same is valid for the crystal growth with an anisotropic surface energy: The larger the surface energy is on a surface with a normal $\mathbf{e}_i$, the larger is also the growth rate in the direction $\mathbf{e}_i$.

The evaluated parameters β are used in the PFM for the simulation of the anisotropy of the MT.

2.6. The change of the habit plane

There are also the observations reported for the $\{2\ 2\ 5\}_F$ transformation (Patterson and Wayman, 1966) revealing that the macroscopic martensitic plate is composed of more fundamental subplates. Hence there is some evidence to suggest that for α' martensitic plates investigated in Sato and Zaefferer (2009) $\{2\ 5\ 9\}_F$ plates are formed from subplates with habit plane $\{2\ 2\ 5\}_F$.

From the morphology analysis carried out by Khachaturyan (1983) we know that the anisotropy of the strain energy function $B(\mathbf{n})$ contributes to the formation of a coherent inclusion shape similar to the anisotropy of the surface energy. The strain energy function of the direction $\mathbf{n}$ is defined as

$$B(\mathbf{n}) = \lambda_{ijkl}\varepsilon_{ij}^0\varepsilon_{kl}^0 - n_i\sigma_{ij}^0\Omega_{jl}^{-1}(\mathbf{n})\sigma_{lm}^0 n_m. \tag{49}$$

In the direction normal to the habit plane $\mathbf{n}_0$ the function (49) is minimal $B(\mathbf{n}_0) = \min B(\mathbf{n})$. In the case when the strain energy function has the same or slightly different values for two crystallographic nonequivalent vectors $\mathbf{n}_0$ and $\mathbf{n}_1$ the situation is more complex. The plane providing the lower surface energy is preferred in that case. The change of the habit

plane orientation from $\mathbf{n}_0$ to $\mathbf{n}_1$ results in the change of the free energy

$$\Delta E = \tfrac{1}{2}(B(\mathbf{n}_1)-B(\mathbf{n}_0))V + 2(\gamma_s(\mathbf{n}_1)-\gamma_s(\mathbf{n}_0))L^2, \tag{50}$$

where γ_s is the surface energy and the volume of an inclusion is equal to $V = DL^2$. The habit plane orientation $\mathbf{n}_1$ will be favored if $\Delta E \le 0$ or

$$D \le \frac{4|\gamma_s(\mathbf{n}_1)-\gamma_s(\mathbf{n}_0)|}{(B(\mathbf{n}_1)-B(\mathbf{n}_0))}. \tag{51}$$

Based on all the individual contributions derived in this section we can now proceed to formulate the full PFM for the butterfly-type martensitic transformation with accommodation dislocations.

3. The PFM for martensitic transformation with accommodation dislocations

3.1. The phase-field formulation

According to the standard definition of phase-field models, an order parameter ϕ represents a property of the system, that is not zero in a region of a phase space and zero otherwise. We define a set of the phase-field variables of the austenite/martensite mixture $\{\phi_p(\mathbf{r})\} = (\phi_1(\mathbf{r}),\dots,\phi_v(\mathbf{r}))$, where $\mathbf{r}$ is the coordinate vector and v is the total number of martensitic orientation variants and $p \in \{1,\dots,v\}$ is an index corresponding to an orientation variant of the martensitic phase. All phase-field variables change in an interval from 0 to 1 and the sum of these variables, including the austenitic phase, on a site $\mathbf{r}$ should be equal to 1. The phase-field variable of austenitic phase is defined as $\phi_A(\mathbf{r}) = 1 - \sum_{p=1}^{v} \phi_p(\mathbf{r})$. The shape function $\eta_p(\mathbf{r})$ used in Section 2 is a function of the phase-field variable $\phi_p(\mathbf{r})$. It interpolates the free energy function between two phases. For computational purposes we chose it so that the minima of the free energy remain at fixed values $\phi_p(\mathbf{r}) = \eta_p(\mathbf{r}) = 0$ in a specific phase labeled by p and $\phi_p(\mathbf{r}) = \eta_p(\mathbf{r}) = 1$ in all other phases (see below Eq. (56)).

The theory of the phase-field evolution is based on the free energy functional of an investigated material system, which consists of the chemical energy and the elastic energy

$$F = \int_V f(\{\phi_p\},T)\,dV + E_{el}. \tag{52}$$

The chemical energy part is given by an integral of the chemical energy density over a representative volume. The chemical energy density can be written as a sum of interface energies and chemical free energies of all phases

$$f(\{\phi_p\},T) = \sum_p f_p(\phi_p,T),$$

$$f_p(\phi_p,T) = \frac{K}{2}(\nabla\phi_p)^2 + Hf_p(\phi_p) + f^{\mathrm{th}}(T)\eta_p(\phi_p). \tag{53}$$

The first term on the right hand side of Eq. (53) is the gradient term. $f_p(\phi_p)$ is the double-well potential function and the function f^{th} is the chemical energy density. The constant H has dimensions of energy per unit volume and the constant K has dimensions of energy per unit length. These constants are responsible for the surface energy defined as $\gamma_s = \sqrt{HK}$.

The chemical energy is related to the undercooling by the relation (Artemev et al., 2001; Turteltaub and Suiker, 2006)

$$f^{\mathrm{th}}(T) = \frac{Q_M(T-T_0)}{T_0} + (S^M - S^A)\left(T\ln\frac{T}{T_0} - (T-T_0)\right), \tag{54}$$

where Q_M is the latent heat of the MT, T_0 is the equilibrium transformation temperature, S^M is the specific heat of martensite and S^A is the specific heat of austenite. For the Fe–Ni system we have chosen $S^M = S^A$.

For our simulation one can choose conventional model functions for $\eta_p(\phi_p)$ and $f(\phi_p)$ according to the standard phase-field models for dendritic growth, see e.g. Karma and Rappel (1998) and Folch and Plapp (2005). This gives the following forms for the double-well potential function

$$f_p(\phi_p) = \phi_p^2(1-\phi_p)^2. \tag{55}$$

and the shape function

$$\eta_p(\phi_p) = \phi_p^3(6\phi_p^2 - 15\phi_p + 10). \tag{56}$$

The dynamics of a phase ϕ_p can now be derived by the minimization of the free energy functional F as a function of a martensitic phase variable ϕ_p and the austenitic phase variable ϕ_A

$$\tau\frac{\partial\phi_p}{\partial t} = -\frac{1}{H}\frac{\delta F(\phi_p,\phi_A)}{\delta\phi_p}. \tag{57}$$

The other phase-field variables are taken to be constant. Here τ is a relaxation time at an interface between the martensitic plate and austenite. The system of kinetic equations for phase fields is the first part of the standard phase-field model.

The second part is the diffusion equation for the temperature field, which in the present model is omitted as negligible in comparison to the elastic part of the energy. The second part of the PFM is now the equation for the evolution of the elastic energy.

The kinetic equation for a martensitic plate with a phase-field variable ϕ_p can be derived using (52), (53) and (57) as

$$\tau\frac{\partial\phi_p(\mathbf{r},t)}{\partial t}=W^2\nabla^2\phi_p(\mathbf{r},t)-f'_p(\mathbf{r},t)-\lambda\eta'_p(\mathbf{r},t)U(\mathbf{r},t), \tag{58}$$

where $W=\sqrt{K/H}$ is the interface thickness, $\lambda=Q^M/H$ is the coupling constant between the phase-field variable and a diffusion field U, $f'_p(\mathbf{r},t)=\partial f_p(\phi_p)/\partial\phi_p$ and $\eta'_p(\mathbf{r},t)=\partial\eta_p(\phi_p)/\partial\phi_p$. We use the phase-field formulation of a two-phase system for the sake of simplicity. The last term in the kinetic equation is the driving force of the MT. The dimensionless variable U is defined as

$$U(\mathbf{r},t)=\frac{T^*(\mathbf{r},t)-T_0}{T_0}, \tag{59}$$

Here T^* is the effective temperature changing due to the elastic effects

$$T^*(\mathbf{r},t)=T+\frac{\Delta G^{\mathrm{el}}(\mathbf{r},t)}{Q^M\eta'_p(\mathbf{r},t)}T_0, \tag{60}$$

where the elastic correction of the driving force is calculated from Eq. (57) as

$$\Delta G^{\mathrm{el}}(\mathbf{r},t)=\frac{\delta E^{\mathrm{el}}(t)}{\delta\phi_p(\mathbf{r},t)}. \tag{61}$$

Note that U is the function of the elastic energy changing during martensitic transformation. The derivation of the elastic term ΔG^{el} in the driving force of the MT will be done in Section 3.3.

3.2. Simulation of the anisotropic kinetics

In this section we take into account the anisotropy of the shape of the martensitic plate described in Section 2.4, and calculated in Section 2.5. First we define a mixture interface energy γ_{mix} as a combination of the surface energy γ_s and the edge elastic energy γ_{edge}. Due to the anisotropy of the surface energy and the elastic contribution the mixture interface energy is also anisotropic. We can write the anisotropic interface energy and the corresponding parameters in the phase-field model as

$$\gamma_{\mathrm{mix}}(\mathbf{n}_{\mathrm{int}})=\gamma_{\mathrm{mix}}a_s(\mathbf{n}_{\mathrm{int}}), \tag{62}$$

$$K(\mathbf{n}_{\mathrm{int}})=Ka_s(\mathbf{n}_{\mathrm{int}}) \tag{63}$$

and

$$H(\mathbf{n}_{\mathrm{int}})=Ha_s(\mathbf{n}_{\mathrm{int}}), \tag{64}$$

where $a_s(\mathbf{n}_{\mathrm{int}})$ is the anisotropic function and

$$\mathbf{n}_{\mathrm{int}}=\frac{\nabla\phi}{|\nabla\phi|} \tag{65}$$

is the normal direction to the interface.

The model parameter H can be defined as

$$H(\mathbf{n}_{\mathrm{int}})=\frac{\gamma_{\mathrm{mix}}(\mathbf{n}_{\mathrm{int}})}{W}=\frac{\gamma_s(\mathbf{n}_{\mathrm{int}})}{W}+\frac{\beta(\mathbf{n}_0,\mathbf{n}_{\mathrm{int}})D}{W}, \tag{66}$$

where $\beta(\mathbf{n}_0,\mathbf{n}_{\mathrm{int}})=\beta_{ij}(\mathbf{n}_0)n_i^{\mathrm{int}}n_j^{\mathrm{int}}$ is a function of the edge elastic energy in units of energy per unit volume and D is the maximal size of the crystal in the direction $\mathbf{n}_0$. In the direction $\mathbf{n}_0$ the edge elastic energy is equal to zero, so that $\beta(\mathbf{n}_0)=0$ and $H(\mathbf{n}_0)=\gamma_s(\mathbf{n}_0)/W$. From Eq. (66) anisotropic function can be defined as

$$a_s(\mathbf{n}_{\mathrm{int}})=1+\frac{\beta(\mathbf{n}_{\mathrm{int}})D}{\gamma_s(\mathbf{n}_{\mathrm{int}})}. \tag{67}$$

Due to the shape dependency of the edge elastic energy the anisotropy function also depends on the width of the martensitic plate D. In the following simulations we assume an isotropic surface energy γ_s.

Since $\beta(\mathbf{e}_1)>\beta(\mathbf{e}_2)\gg\gamma_s/D$ (see Section 2.5) we can assume the limits $a_s(\mathbf{e}_1)=\beta_1D/\gamma_s$, $a_s(\mathbf{e}_2)=\beta_2D/\gamma_s$ and $a_s(\mathbf{e}_3)=\beta_3D/\gamma_s$ with $\beta_3=\gamma_s/D$ and write the anisotropic function through eigenvalues β_i and eigenvectors $\mathbf{e}_i$ in the following form:

$$a_s(\mathbf{n}_{\mathrm{int}})=\sum_i\frac{\beta_i}{\beta_1}(\mathbf{n}_{\mathrm{int}}\cdot\mathbf{e}_i)^2. \tag{68}$$

The kinetic equation is obtained by

$$\tau\frac{\partial\phi_p}{\partial t}=-\frac{1}{H(\mathbf{n}_{\rm int}^{\perp})}\frac{\delta F(K(\mathbf{n}_{\rm int}^{\perp}),\phi_p,\phi_A)}{\delta\phi_p}, \tag{69}$$

where the normal to the growth direction $\mathbf{n}_{\rm int}^{\perp}$ expresses the fact that the formation of a surface plane with normal $\mathbf{n}_{\rm int}^{\perp}$ effects the growth rate in the direction $\mathbf{n}_{\rm int}$.

Inserting a_s in Eq. (69) we obtain

$$\begin{aligned}\tau a_s(\mathbf{n}_{\rm int}^{\perp})\frac{\partial\phi_p(\mathbf{r},t)}{\partial t}&=W^2\Big(\boldsymbol{\nabla}\cdot[a_s(\mathbf{n}_{\rm int}^{\perp})\boldsymbol{\nabla}\phi_p(\mathbf{r},t)]+\partial_x\Big(|\boldsymbol{\nabla}\phi_p|^2a_s(\mathbf{n}_{\rm int}^{\perp})^{1/2}\frac{\partial a_s(\mathbf{n}_{\rm int}^{\perp})^{1/2}}{\partial(\partial_x\phi_p)}\Big)\\&+\partial_y\Big(|\boldsymbol{\nabla}\phi_p|^2a_s(\mathbf{n}_{\rm int}^{\perp})^{1/2}\frac{\partial a_s(\mathbf{n}_{\rm int}^{\perp})^{1/2}}{\partial(\partial_y\phi_p)}\Big)+\partial_z\Big(|\boldsymbol{\nabla}\phi_p|^2a_s(\mathbf{n}_{\rm int}^{\perp})^{1/2}\frac{\partial a_s(\mathbf{n}_{\rm int}^{\perp})^{1/2}}{\partial(\partial_z\phi)_p}\Big)\Big)-f_p'a_s(\mathbf{n}_{\rm int}^{\perp})-\lambda\eta_p'U.\end{aligned} \tag{70}$$

To avoid the arbitrary choice of $\mathbf{n}_{\rm int}^{\perp}$ in 3D-simulation we suggest to assume

$$a_s(\mathbf{n}_{\rm int}^{\perp})=a_s^{-1}(\mathbf{n}_{\rm int}). \tag{71}$$

Since we have a large anisotropy parameter for the directions normal to the habit plane, we can simplify the model and make a pseudo-2D simulation. For this aim we use the following procedure: (i) the initial coordinate is chosen with x-, y- and z-axes being parallel to the directions $\langle 1\,0\,0\rangle_\gamma$, $\langle 0\,1\,0\rangle_\gamma$ and $\langle 0\,0\,1\rangle_\gamma$ of an austenitic crystal; (ii) all coordinates and parameters such as the eigenstrain tensor and strain energy functions transform to the Cartesian coordinate system (x', y', z') corresponding to a martensitic variant with eigenvectors $\mathbf{e}_1$, $\mathbf{e}_2$ and $\mathbf{e}_3$ (the habit plane $\mathbf{n}_0=\mathbf{e}_3$ is parallel to the z'-axis); (iii) the kinetic equation is solved in the new coordinate system in two dimensions (x', y'); (iv) the coordinates are transformed to the initial Cartesian coordinate system. After that the elastic energy and the evolution of the accommodation dislocation (see Section 3.4) are calculated in 3D space, this is iteratively repeated from item (ii).

The kinetic equation is calculated in the plane, which is parallel to the habit plane and passes the point of the formation of a martensitic nucleus. The transformation matrix from the system (x', y', z') with the basis $(\mathbf{e}_1, \mathbf{e}_2, \mathbf{e}_3)$ to the system (x, y, z) with the basis $(\langle 1\,0\,0\rangle_\gamma, \langle 0\,1\,0\rangle_\gamma, \langle 001\rangle_\gamma)$ is defined as

$$\hat{\mathbf{T}}(\mathbf{n})=\begin{pmatrix}\cos\kappa & \cos\theta\sin\kappa & \sin\theta\sin\kappa\\ -\sin\kappa & \cos\theta\cos\kappa & \sin\theta\cos\kappa\\ 0 & -\sin\theta & \cos\theta\end{pmatrix}. \tag{72}$$

After the substitution of the habit plane $\mathbf{n}_0=(n_1,n_2,n_3)$ we have

$$\hat{\mathbf{T}}(\mathbf{n})=\begin{pmatrix}\frac{n_2}{\sqrt{1-n_3^2}} & \frac{n_3n_1}{\sqrt{1-n_3^2}} & n_1\\ -\frac{n_1}{\sqrt{1-n_3^2}} & \frac{n_3n_2}{\sqrt{1-n_3^2}} & n_2\\ 0 & -\sqrt{1-n_3^2} & n_3\end{pmatrix}. \tag{73}$$

Back transformation proceeds by

$$(x\ y\ z)^T=\hat{\mathbf{T}}^{-1}(x'\ y'\ z')^T. \tag{74}$$

3.3. The calculation of the elastic component in the driving force of the martensitic transformation

To calculate the elastic component in the driving force of the MT we now consider the part of the elastic energy

$$\tilde{E}^{\rm el}=E^{\rm el}-E^{\rm self}_{\rm edge}. \tag{75}$$

The edge part of the self-energy of the martensitic plate is taken into account in the anisotropic formulation.

Then the elastic component in driving force is calculated for two variants of the MT from Eq. (22) as

$$\begin{aligned}\Delta G^{\rm el}=\delta\frac{\tilde{E}^{\rm el}(t)}{\delta\phi_p(\mathbf{r},t)}&=B_{pp}(\mathbf{n_0})(\eta_p(\mathbf{r})-\langle\eta_p\rangle)\eta_p'(\mathbf{r},t)+\eta_p'(\mathbf{r},t)\fint\frac{\mathrm{d}^3\mathbf{k}}{(2\pi)^3}B_{pq}(\mathbf{n})e^{i\mathbf{kr}}\widehat{\eta}_q(\mathbf{k})\\&+\eta_p'(\mathbf{r},t)\sum_{\alpha=1}^{\mu}\fint\frac{\mathrm{d}^3\mathbf{k}}{(2\pi)^3}B_{p\alpha}(\mathbf{n})e^{i\mathbf{kr}}\widehat{\phi}_\alpha^d(\mathbf{k})+\eta_p'(\mathbf{r},t)\sum_{\alpha=1}^{\mu}\fint\frac{\mathrm{d}^3\mathbf{k}}{(2\pi)^3}B_{\alpha p}(\mathbf{n})e^{i\mathbf{kr}}\widehat{\phi}_\alpha^d(\mathbf{k})\\&+\eta_p'(\mathbf{r},t)\sum_{\alpha,\beta=1}^{\mu}\frac{\partial\phi_\alpha^d(\mathbf{r})}{\partial\phi_p(\mathbf{r})}\fint\frac{\mathrm{d}^3\mathbf{k}}{(2\pi)^3}B_{\alpha\beta}(\mathbf{n})e^{i\mathbf{kr}}\widehat{\phi}_\alpha^d(\mathbf{k}).\end{aligned} \tag{76}$$

In the last term we take into account that the function ϕ_α^d of the dislocation density depends on the phase-field variable ϕ_p, as it can be seen below from Eq. (91).

In our simulations we neglect the interaction of the edge elastic energy of a particle with a second martensitic plate as well as with the accommodation dislocations. These simplifications are underlying the formulation of Eq. (76):

$$\Delta G^{\mathrm{el}} = \delta \frac{\tilde{E}^{\mathrm{el}}(t)}{\delta \phi_p(\mathbf{r},t)} = B_{pp}(\mathbf{n_0})(\eta_p(\mathbf{r}) - \langle \eta_p \rangle)\eta_p'(\mathbf{r},t) + B_{pq}(\mathbf{n_0})(\eta_q(\mathbf{r}) - \langle \eta_q \rangle)\eta_p'(\mathbf{r},t) + \sum_{\alpha=1}^{\mu} B_{p\alpha}(\mathbf{n_0})(\phi_\alpha^d(\mathbf{r}) - \langle \phi_\alpha^d \rangle)\eta_p'(\mathbf{r},t) + \sum_{\alpha=1}^{\mu} B_{\alpha p}(\mathbf{n_0})(\phi_\alpha^d(\mathbf{r}) - \langle \phi_\alpha^d \rangle)\eta_p'(\mathbf{r},t) + \sum_{\alpha,\beta=1}^{\mu} \frac{\partial \phi_\alpha^d(\mathbf{r})}{\partial \phi_p(\mathbf{r})} B_{\alpha\beta}(\mathbf{n_0})(\phi_\alpha^d(\mathbf{r}) - \langle \phi_\alpha^d \rangle)\eta_p'(\mathbf{r},t). \tag{77}$$

The first term in Eq. (76) and all terms in Eq. (77) are obtained using the Parseval theorem (see also Khachaturyan, 1983). For example the second term in Eq. (22) for a constant $\mathbf{n_0}$ transforms to

$$\oint \frac{\mathrm{d}^3\mathbf{k}}{(2\pi)^3} B_{pq}(\mathbf{n_0})\widehat{\eta}_p(\mathbf{k})\widehat{\eta}_q(\mathbf{k}) = B_{pq}(\mathbf{n_0}) \int \frac{\mathrm{d}^3\mathbf{k}}{(2\pi)^3} \Delta\widehat{\eta}_p(\mathbf{k})\Delta\widehat{\eta}_q(\mathbf{k}) = B_{pq}(\mathbf{n_0}) \int \Delta\eta_p(\mathbf{r})\Delta\eta_q(\mathbf{r})\, d\mathbf{r}. \tag{78}$$

From Eq. (77) it can be seen that the accommodation dislocations play a crucial role in the transformation kinetic. The last terms in the driving force increase with increasing dislocation density, that leads to a decreasing effective temperature and at $T^* = T_0$ to the termination of the transformation process. In their experimental work Sato and Zaefferer (2009) conjectured that most likely the transformation process comes to an end when the austenitic phase is that much strain-hardened that its further deformation is no longer possible.

Based on the estimation of the equilibrium shape of the single martensitic plate and the elastic part of the driving force we can now simulate the evolution of the phase-field variable of a martensitic phase, taking into account the interplay of all kinetic and energetic contributions. As a result we can determine the influence of the individual contributions on the final morphology that will arise after any kind of mechanically induced transformation accompanied by accommodation dislocations.

3.4. The evolution of the accommodation dislocation density

In this section we describe the time evolution of the density of the accommodation dislocations generated during the MT and forming plastic deformation strain outlined in Section 2.2.

In order to determine the evolution of the dislocation density we define the mobile dislocation density $\rho_{\mathrm{M},\alpha}$, the immobile dislocation density $\rho_{\mathrm{I},\alpha}$, the parallel dislocation density $\rho_{\mathrm{P},\alpha}$ and forest dislocation density $\rho_{\mathrm{F},\alpha}$ for a slip system α. Following Ma and Roters (2004) we define

$$\rho_{\mathrm{F},\alpha} = \sum_{\beta=1}^{N} \rho_{\mathrm{I},\beta} |\cos(\mathbf{n}^{(\alpha)}, \mathbf{n}^{(\beta)} \times \mathbf{m}^{(\beta)})|, \tag{79}$$

$$\rho_{\mathrm{P},\alpha} = \sum_{\beta=1}^{N} \rho_{\mathrm{I},\beta} |\sin(\mathbf{n}^{(\alpha)}, \mathbf{n}^{(\beta)} \times \mathbf{m}^{(\beta)})|, \tag{80}$$

$$\rho_{\mathrm{M},\alpha} \approx \frac{2k_{\mathrm{B}}T}{c_1 c_2 c_3 G b_\alpha^3} \sqrt{\rho_{\mathrm{F},\alpha}\rho_{\mathrm{P},\alpha}}, \tag{81}$$

where G is the shear modulus, k_{B} is the Boltzmann constant, T is the temperature and c_1, c_2, c_3 are numerical constants. Using the Orowan theory we can calculate the evolution of the dislocation density of the immobile dislocations by

$$\dot{\rho}_{I,\alpha} = c_4 \sqrt{\rho_{\mathrm{F},\alpha}}\dot{\gamma}, \tag{82}$$

where the evolution of the average slip velocity of the dislocation lines is defined as

$$\dot{\gamma}_\alpha = \rho_{M,\alpha} b_\alpha v_\alpha \phi_A. \tag{83}$$

Here we assume that transformation-induced plastic deformation is hindered in the martensite owing to its much high flow stress compared to the austenite and, hence, we describe the evolution of plastic slip during the process only in the austenitic phase. This assumption is consistent with the plastic deformation accumulation that was experimentally observed in the original work of Sato and Zaefferer (2009).

The average dislocation velocity can be found based on the model of thermally activated dislocation motion as (Ma and Roters, 2004; Roters et al., 2000)

$$v_\alpha = \lambda_\alpha \nu_\alpha \exp\left(-\frac{Q_{\mathrm{slip}}}{k_{\mathrm{B}}T}\right) \sinh\left(\frac{|\tau_\alpha| - \tau_{\mathrm{pass},\alpha}}{k_{\mathrm{B}}T} V_\alpha\right) \tag{84}$$

with

$$\tau_\alpha \cong \hat{\sigma} \cdot \hat{\mathbf{M}}_\alpha \tag{85}$$

being the external stress or the external driving force and

$$\tau_{\mathrm{pass},\alpha} = c_1 G b_\alpha \sqrt{\rho_{\mathrm{P},\alpha} + \rho_{\mathrm{M},\alpha}} \tag{86}$$

being the stress of the mobile dislocations, where v_α is the attack frequency, Q_{slip} is the effective activation energy for the dislocation slip, $\hat{\sigma}$ is the external stress. The jump width λ_α and the activation volume V_α are calculated as

$$\lambda_\alpha = \frac{c_2}{\sqrt{\rho_{F,\alpha}}} \tag{87}$$

and

$$V_\alpha = c_3 b_\alpha^2 \lambda_\alpha, \tag{88}$$

where c_2 and c_3 are constants.

Now we show that the external driving force of the dislocation evolution (85) can be derived from the total elastic energy (22). The components of the stress tensor can be defined from the total elastic energy

$$(\hat{\boldsymbol{\sigma}})_{ij} = \sum_{p=1}^{v} \frac{\partial E_{\mathrm{elast}}}{\partial \varepsilon_{ij}^0(p,\mathbf{r})}, \tag{89}$$

where $\varepsilon_{ij}^0(p,\mathbf{r}) = \varepsilon_{ij}^0(p)\eta_p(\mathbf{r})$. After differentiation of Eq. (22) we obtain

$$\begin{aligned}(\hat{\boldsymbol{\sigma}})_{ij} = {} & \frac{1}{2}\sum_{q=1}^{v} \fint \frac{\mathrm{d}^3\mathbf{k}}{(2\pi)^3} [\lambda_{ijkl}\varepsilon_{kl}^0(q) - n_i\lambda_{ijkl}\Omega_{jk}(\mathbf{n})\lambda_{klij}\varepsilon_{kl}^0(q)n_l]\widehat{\eta}_q(\mathbf{k})\mathrm{e}^{i\mathbf{kr}} \\ & - \frac{1}{2}\sum_{\alpha=1}^{\mu} \fint \frac{\mathrm{d}^3\mathbf{k}}{(2\pi)^3} [\lambda_{ijkl}M_{kl}(\alpha) - n_i\lambda_{ijkl}\Omega_{jk}(\mathbf{n})\lambda_{klij}M_{kl}(\alpha)n_l]\widehat{\phi}_\alpha^{\,d}(\mathbf{k})\mathrm{e}^{i\mathbf{kr}}.\end{aligned} \tag{90}$$

Inserting the stress tensor in Eq. (85) we can write the external stress as

$$\tau_\alpha = \frac{1}{2}\sum_{q=1}^{v} \fint \frac{\mathrm{d}^3\mathbf{k}}{(2\pi)^3} B_{\alpha q}(\mathbf{n})\widehat{\eta}_q(\mathbf{k})\mathrm{e}^{i\mathbf{kr}} - \frac{1}{2}\sum_{\beta=1}^{\mu} \fint \frac{\mathrm{d}^3\mathbf{k}}{(2\pi)^3} B_{\alpha\beta}(\mathbf{n})\widehat{\phi}_\beta^{\,d}(\mathbf{k})\mathrm{e}^{i\mathbf{kr}}. \tag{91}$$

4. Numerical simulation

4.1. Simulation scheme

In this section we demonstrate how the model derived in the previous sections is applied in numerical simulations. The complete set of evolution equations for our model consists of two parts which are the phase-field part and the dislocation evolution part as it is shown in Fig. 3. In the phase-field part we calculate two kinetic equations for two variants of the MT. They are given by Eq. (70) and include a contribution of the elastic energy to the driving force given by Eq. (76), as well as the anisotropy function equation (68). The dislocation evolution part consists of the set of equations (79)–(88) with external driving force equation (91) (see Section 3.4).

To arrive at a numerical efficient formulation we can reduce the complexity of the above set of coupled equations ass follows by inserting Eqs. (83)–(88) into (82). This yields the following set of equations for the evolution of immobile dislocation densities:

$$\dot{\rho}_{I,\alpha} = \rho_{M,\alpha} b^{(\alpha)} c_4 c_2 v_\alpha \phi_A \exp\left(-\frac{Q_{\mathrm{slip}}}{k_B T}\right) \sinh\left(\frac{\kappa Q_{\mathrm{slip}}}{k_B T}\right) \tag{92}$$

with

$$\kappa = \frac{\left(|\tau_\alpha| - c_1 G b^{(\alpha)} \sqrt{\rho_{P,\alpha} + \rho_{M,\alpha}}\right)}{c_1 G b^{(\alpha)} \sqrt{\rho_{F,\alpha}}} \cdot 2c_1 c_2 c_3, \tag{93}$$

where the dislocation densities $\rho_{P,\alpha}$, $\rho_{F,\alpha}$ and $\rho_{M,\alpha}$ are defined by Eqs. (79)–(81). The external stress is given by Eq. (91). Here we use the fact that the effective activation energy for dislocation slip is equal to $Q_{\mathrm{slip}} = 1/2Gb^3$. Eq. (92) must be stepwise integrated in each time step.

Successive to the solution of the evolution equation for the dislocation density (92) the following coupling equation is applied for the calculation of the dislocation slip function:

$$\phi_\alpha^d(\mathbf{r},t) = b^{(\alpha)} \sqrt{(\rho_{I,\alpha}(\mathbf{r},t) + \rho_{M,\alpha}(\mathbf{r},t))}. \tag{94}$$

In the simulation we assume $a \ll 1/\sqrt{\rho_d}$ and omit the energy of dislocation core. The two differential equations, which constitute our model (Eq. (70) for the phase-field evolution and Eq. (92) for the dislocation density evolution), are

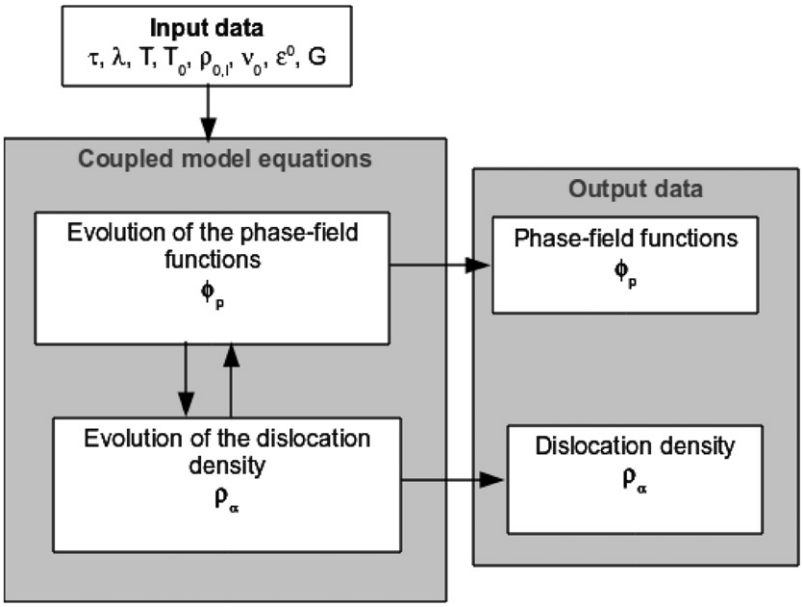

Fig. 3. The simulation scheme. The following input parameters are presented: the kinetic parameter τ, the coupling constant λ, the temperature T_0 of the MT, the initial dislocation density $\rho_{0,i}$, the attack frequency ν_α, the eigenstrain matrix of the MT ε^0, the shear modulus G.

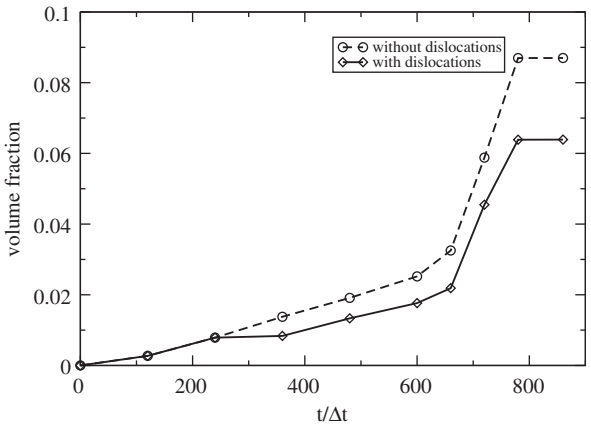

Fig. 4. The simulated transformation curves obtained with and without accommodation dislocations. The total martensitic volume fraction in the simulated domain is calculated.

numerically integrated by using a simple Euler, forward-time finite difference scheme. For the Laplacian we employ a nine-point formula involving nearest and next nearest neighbors. Our simulations are carried out on a 3D domain of size $150 \times 150 \times 150\ \Delta x$ with periodic boundary conditions.

4.2. Model parameters

In the phase-field part of the model we have chosen the following input parameters: the interface thickness $W = \Delta x = 7.0 \times 10^{-7}$ m, the latent heat $Q_M = 3.5 \times 10^8$ J m^{-3} (Artemev et al., 2001), the surface energy $\gamma_s = 1.9$ J m^{-2} for $\{2\ 5\ 2\}_\gamma$ plane and $\gamma_s = 2.5$ J m^{-2} for $\{2\ 9\ 5\}_\gamma$ (Kuznetsov et al., 1998). From the chosen parameters the coupling constant $\lambda = Q_M W/\gamma_s$ is 130 and 100 respectively.

For our simulations we assume a transformation law from the experimental data (Tjahjanto et al., 2008) with the maximal transformation rate $\dot{\xi}_0 = 0.003$ s^{-1}. Here the transformation rate is defined as the mean rate of the martensitic transformation averaged over the whole system, taking into account the dynamical constraints imposed by crystal defects as well as the nucleation of new plates. From this value we have estimated the mean transformation rate for our case as 0.3 s^{-1} and the corresponding kinetic parameter as $\tau = 3$ s taking into account the anisotropy ($D/L \cong 0.01$). From these

kinetic parameters the time step of the simulation is chosen as $\Delta t = 0.005\tau$, which is smaller than the stability limit $\Delta t < \tau/\lambda$.

The following material parameters for the simulated Fe–30 wt%Ni alloy are underlying the simulation results, which we present in the following: shear modulus $G = 0.84$ GPa, the lattice constant $a = 3.59 \times 10^{-10}$ m, constants $c_1 = 0.18$, $c_2 = 5.0$, $c_3 = 5.0$, $c_4 = 8.0 \times 10^6$ m^{-1}, the initial dislocation density $\rho_{0,I} = 10^8$ m^{-2} for all systems and the attack frequency $v_\alpha = 10^{10}$ s^{-1}. In the fcc lattice of the austenitic matrix 24 variants of the dislocation slip have been chosen with slip plane of type $\{1\,1\,1\}_\gamma$ and the slip direction of type $\langle 1\,0\,1 \rangle_\gamma$.

In the work Umemoto et al. (1983), the temperature of martensitic transformation M_s in the Fe–30 wt%Ni alloy is estimated around the room temperature $T_M = 300$ K. The simulations are carried out under isothermal conditions at an initial undercooling being $(T_0 - T)/T_0 = 0.3$ with $T_0 = 500$ K. Then simulations proceeded with the increasing undercooling $(T_0 - T)/T_0 = 0.5$.

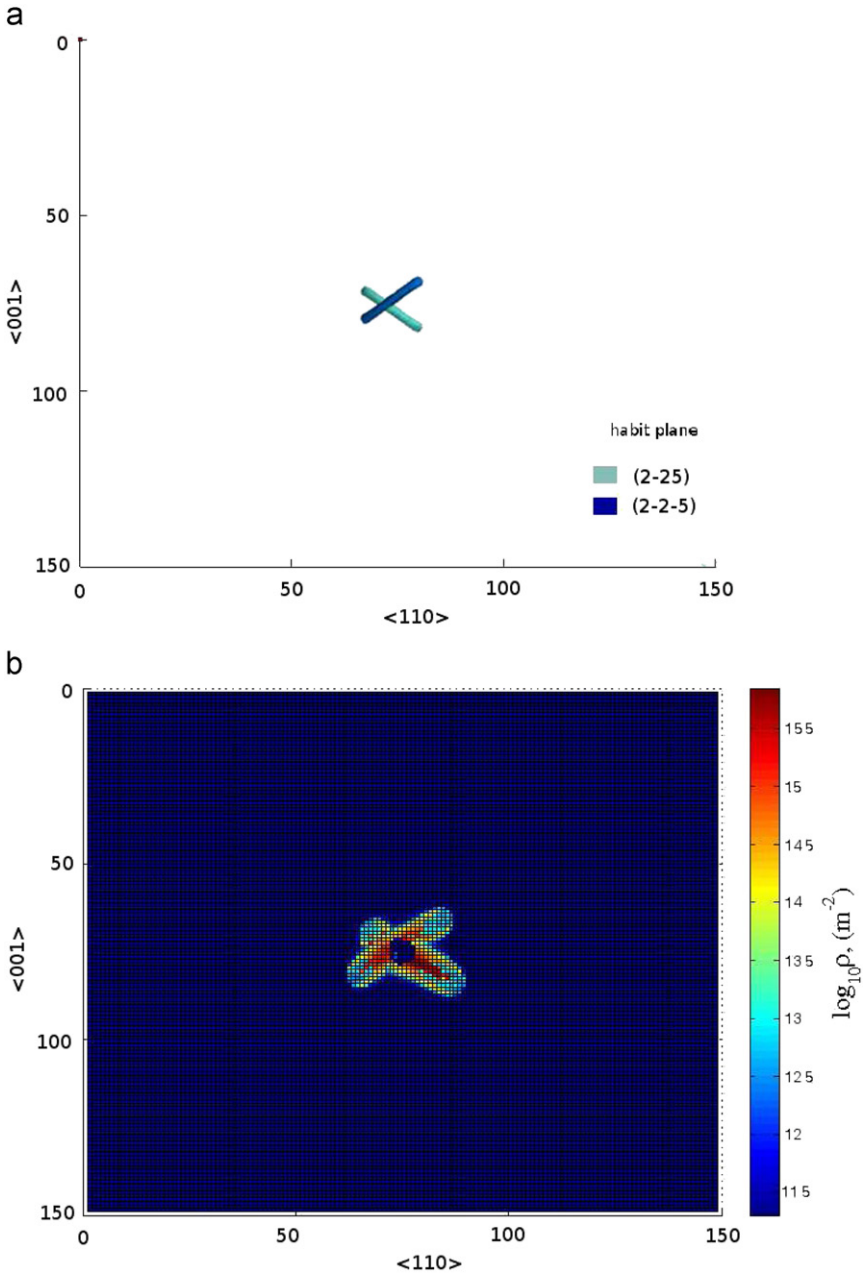

Fig. 5. Simulated micro-structure (a) and the dislocation density around the martensitic plates (b) at $t = 0.9\tau$. (For interpretation of the references to color in this figure legend, the reader is referred to the web version of this article.)

For the two variants of the MT with the habit planes $(2\,\overline{2}\,\overline{5})_\gamma$ and $(2\,\overline{2}\,5)_\gamma$ we use the eigenstrains (Section 2)

$$\varepsilon^0_{ij}(1)=\begin{pmatrix} 0 & -0.0286 & -0.0399 \\ -0.0286 & -0.0838 & -0.1155 \\ 0.0320 & 0.0928 & 0.1294 \end{pmatrix},$$

$$\varepsilon^0_{ij}(2)=\begin{pmatrix} -0.0838 & -0.0286 & -0.1155 \\ -0.0286 & 0 & -0.0399 \\ 0.0928 & 0.0320 & 0.1294 \end{pmatrix}. \tag{95}$$

The corresponding eigenvectors of the matrix $\hat{\boldsymbol{\beta}}$ are

$$e_1(1)=(0.5773\ \ -0.5773\ \ 0.5773),\quad e_2(1)=(0.7035\ \ 0.7035\ \ 0.0),$$

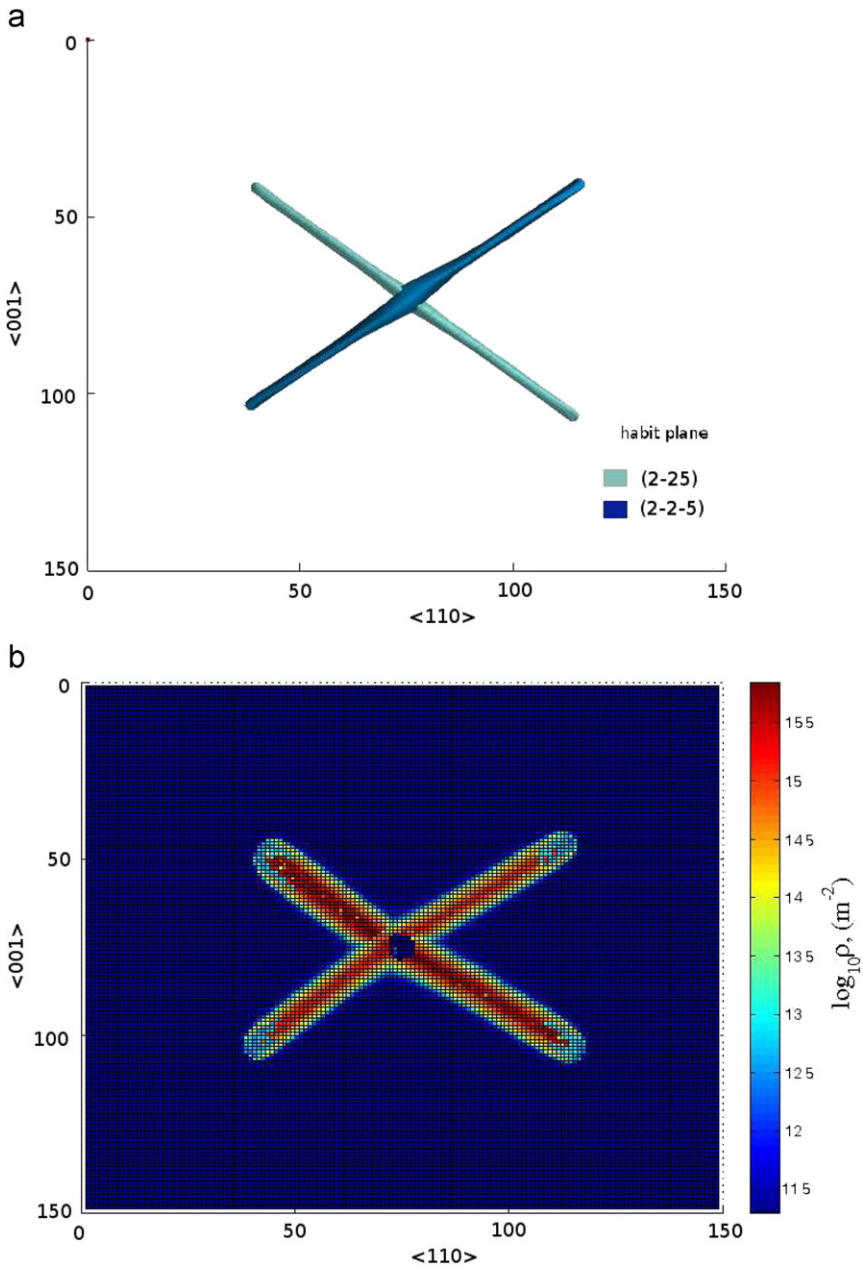

Fig. 6. Simulated micro-structure (a) and the dislocation density around the martensitic plates (b) at $t=3\tau$. (For interpretation of the references to color in this figure legend, the reader is referred to the web version of this article.)

$$e_1(2) = (0.5773\ \ -0.5773\ \ -0.5773), \quad e_2(2) = (0.7035\ \ 0.7035\ \ 0.0). \tag{96}$$

During the transformation the habit plane $(2\,\overline{2}\,\overline{5})_\gamma$ changes to $(2\,\overline{5}\,9)_\gamma$ and $(\overline{2}\,5\,9)_\gamma$ with the eigenvectors

$$e_1(5) = (0.5585\ \ 0.7311\ \ 0.3858), \quad e_2(6) = (0.8165\ \ 0.4082\ \ 0.4082),$$

$$e_1(5) = (0.5585\ \ 0.7311\ \ -0.3858), \quad e_2(6) = (0.8165\ \ 0.4082\ \ -0.4082). \tag{97}$$

The habit plane $(2\,\overline{2}\,5)_\gamma$ changes to $(\overline{5}\,2\,\overline{9})_\gamma$ and $(5\,\overline{2}\,\overline{9})_\gamma$ with

$$e_1(3) = (-0.7311\ \ -0.5585\ \ 0.3858), \quad e_2(3) = (-0.4082\ \ -0.8165\ \ 0.4082),$$

$$e_1(4) = (0.7035\ \ 0.5585\ \ 0.3858), \quad e_2(4) = (0.4082\ \ 0.8165\ \ 0.4082). \tag{98}$$

For the calculation of the anisotropy function the eigenvalues β_1 and β_2 were chosen for the habit plane $\{2\,9\,5\}_F$ and $\{2\,5\,2\}_F$ the same as in Section 2.5. For the value β_3 we assume the relation γ_s/D.

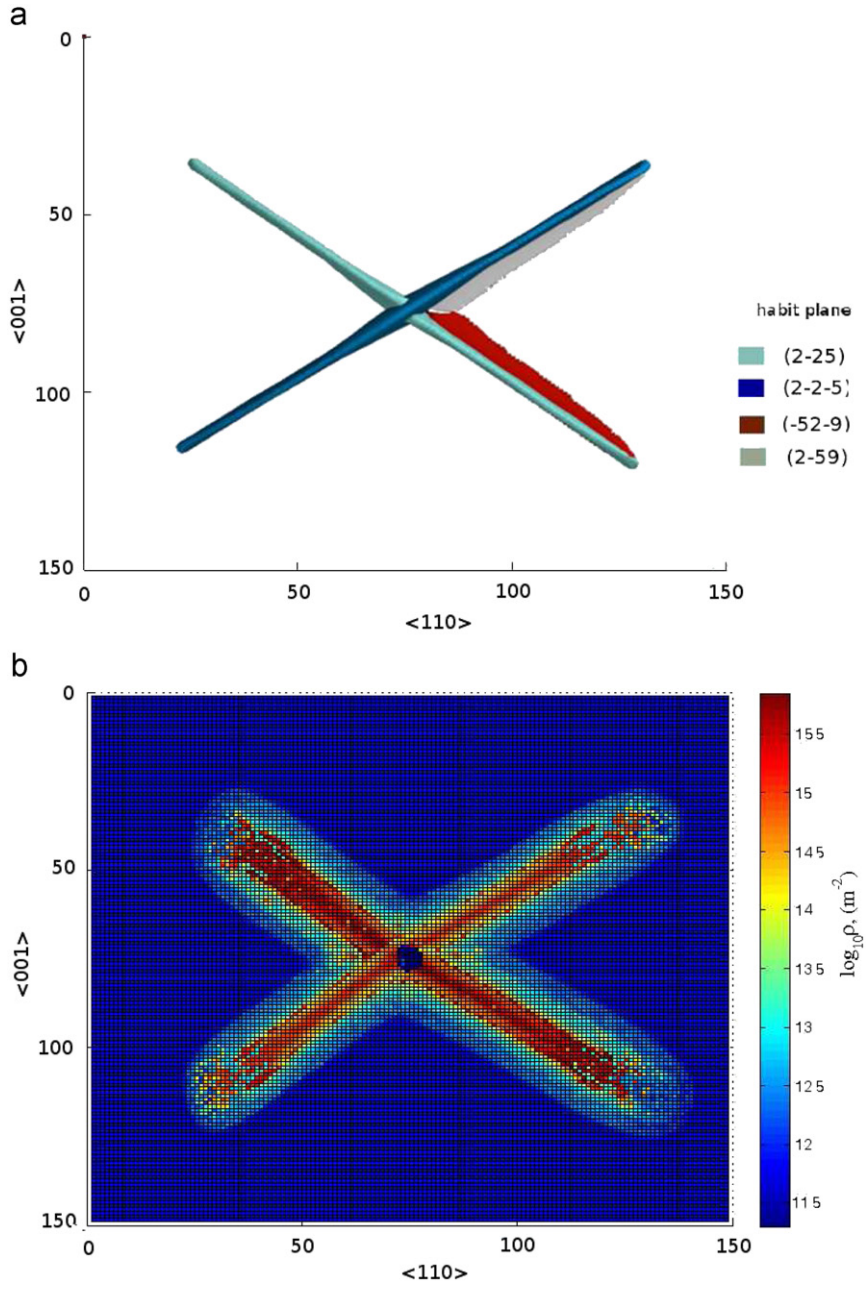

Fig. 7. Simulated micro-structure (a) and the dislocation density around the martensitic plates (b) at $t = 3.9\tau$.

4.3. Results of the simulation and the comparison to the experiment

The nucleation of two martensitic variants occurs in a single austenitic crystal. The size of nuclei of the martensitic phase was chosen as $2\Delta x$. The first nucleus forms in the center of the simulation box, whereas the second one forms on the neighboring sites.

To study the effect of accommodation dislocations on the butterfly-type martensite microstructure the simulation have been performed for two cases with and without dislocations. The simulated transformation curves for these cases are shown in Fig. 4.

In the simulation two martensitic plates start to grow with habit planes $(2\ 2\ 5)_\gamma$ and $(\bar{2}\ \bar{2}\ 5)_\gamma$. The transformation stops at the time 3τ due to the increasing size of the crystals and the increasing mean dislocation density in the system. The microstructure at the time 0.9τ and 3τ is shown in Figs. 5(a) and 6(a). Blue and green colors correspond to the two crystals. We can observe that the two thin lamella grow in main directions according to the anisotropy parameters and cross each other. The dislocation density distribution in the system in the same periods of time is shown in Figs. 5(b) and 6(b).

Then the temperature is lowed and the transformation proceeds. In the case without dislocations the martensitic plates grow up to the boundary of the simulation box and broader keeping the habit plane of type $\{2\ 5\ 2\}_\gamma$. In the second case with dislocation effects the transformation proceeds with the change of habit planes to the new habit planes of type $\{2\ 5\ 9\}_\gamma$. The first habit plane $\{2\ 5\ 2\}_\gamma$ serves as a substrate for the nucleation of new plates. In our simulations nuclei of new martensitic variants of size $2\Delta x$ were inserted at the inner surface of twin-related martensitic plates. The rate of spontaneous nucleation were 1 nucleus per time step for 20 time steps. Then the transformation stops again when the martensitic crystals increase their thickness and fill the volume between old and new habit planes. The mean dislocation density also increases and hinders the further transformation process.

The final microstructure at $t = 3.9\tau$ is shown in Fig. 7(a). The corresponding dislocation density distribution is shown in Fig. 7(b). To show the full intrinsic structure of the martensitic crystals Mayavi2 software is used in Fig. 8. Here the

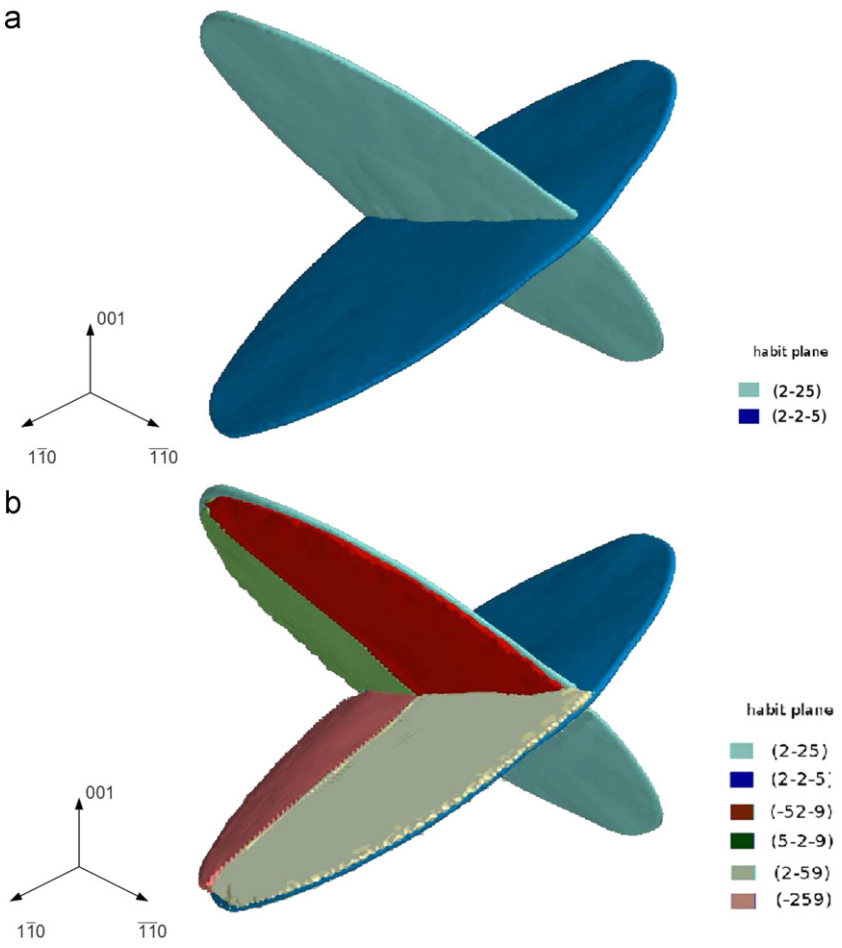

Fig. 8. The simulated microstructure at $t = 3\tau$ (a) and 3.9τ (b) in 3D-plot. The areas with various habit planes are shown by the various colors. (For interpretation of the references to color in this figure legend, the reader is referred to the web version of this article.)

Table 1
The size of the martensitic plate. The comparison of the simulation and the experiment.

Direction	Simulation (μm)	Experiment (μm)
⟨1 1 1⟩	70.5	70.0
⟨1 0 1⟩	25.0	–
⟨2 5 2⟩	7.2	7.0

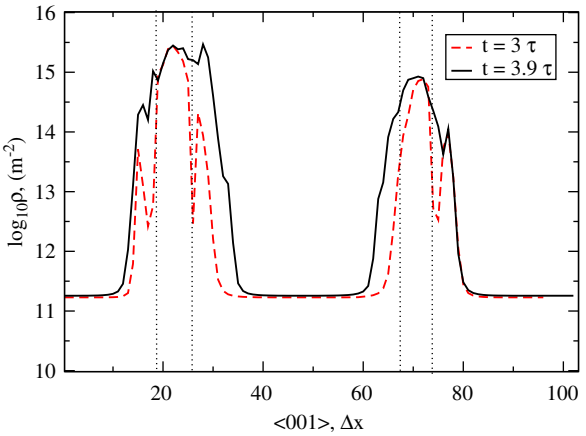

Fig. 9. The dislocation density in the direction [0 0 1] at $t=3\tau$ and $t=3.9\tau$.

simulated structure is shown as 3D-plot. The areas with different habit plane orientation are indicated by the various colors. The butterfly-type martensitic system consists of two crystals. Each crystal contains three distinct regions. One region is a thin lamella with habit plane $\{2\ 5\ 2\}_\gamma$. The other two regions have a three-angular shape with habit plane of type $\{2\ 9\ 5\}_\gamma$.

From these simulation results we can draw the following conclusion: The suggestion, that the transformation process terminates when the austenitic matrix is very much strain hardened (Sato and Zaefferer, 2009), is confirmed in the simulation for the first and for the second part of the transformation. Moreover, the transformation process comes to its end when the equilibrium of elastic energy and chemical energy is reached.

A more detailed comparison of our simulations to experiments yields the following: First, the size of the larger martensitic plate obtained from our 3D simulations is compared to the corresponding experimental values (see Fig. 1) in Table 1. We observe very good qualitative agreement, which validates our model at this point.

Further, the distribution of the dislocation density in the direction $[0\ 0\ 1]_\gamma$ is depicted in Fig. 9. It can be observed that the dislocation density reaches its maximum value on the martensite/austenite interface. The value of dislocation density varies from 5×10^{11} in the volume far from the martensitic crystal to 5×10^{15}. The distribution of the dislocations around the crystals and the size of the first and the second martensitic plates in one system are not equal due to the interplay of the various slip systems.

The comparison of the experimental results presented in Calcagnotto et al. (2010) and our simulated dislocation density profiles yields again excellent agreement and serves as a further model validation.

5. Conclusions

In the present study the formation mechanism of butterfly-type martensite in a Fe–30 wt%Ni alloy was investigated in detail by means of the phase-field model. As the input we have used the anisotropy parameters evaluated from the crystallography of the MT. While the growth of the martensitic phase volume was driven by the chemical free energy reduction, the anisotropy of the microstructure evolution was caused by the anisotropic feature of the elastic energy.

Our new model takes into account the formation of accommodation dislocations in austenitic matrix and their inheritance to the martensitic plates. It resolves the effects of the accommodation dislocations' dynamics on the kinetic of growth as well as on the microstructure.

Comparison between simulations based on our model and experiments yields excellent agreement with experiments for a large number of details characterizing the butterfly type MT.

The thereby developed and validated phase-field model constitutes a general simulation approach which can efficiently resolve different kinds of dislocation dynamics in phase-change materials undergoing mechanical transformations inherently coupled to the kinetics of the transformation process. It reaches far beyond equilibrium crystallography in

the sense that it allows to predict not only the aspect ratio of resulting martensitic crystals, but also the size of the crystals itself, as well as the resulting dislocation distribution. As an outlook, we also intend to investigate in more detail the influence of dislocations on the shape of the growing crystal and to include a description of crystal defects as vacancies and inclusions in our model and study their effect on resulting microstructure evolution.

Acknowledgment

We gratefully acknowledge Joao Rezende RWTH Aachen University for the fruitful discussions and scientific support.

References

Artemev, A., Jin, Y.M., Khachaturyan, A.G., 2001. Acta Mater. 49, 1165.
Artemev, A., Jin, Y.M., Khachaturyan, A.G., 2002. Philos. Mag. A 82, 1249–1270.
Bhadeshia, H.K.D.H., 2001. Worked Examples in the Geometry of Crystals, 2nd ed. Institute of Materials, London.
Breedis, J.F., Wayman, C.M., 1962. Trans. AIME 224, 1128.
Calcagnotto, M., Ponge, D., Demir, E., Raabe, D., 2010. Materials Science and Engineering, A 527 (10–11), 2738–2746.
Chen, L.Q., Wang, Y., Khachaturyan, A.G., 1992. Philos. Mag. Lett. 65, 15–23.
Folch, R., Plapp, M., 2005. Phys. Rev. E 72, 011602.
Gaubert, A., Le Bouar, Y., Finel, A., 2010. Philos. Mag. 90, 375–404.
Hausch, G., Warlimont, H., 1973. Acta Metall. 21, 401–414.
Hu, S.Y., Chen, L.Q., 2001. Acta Mater. 49 (3), 463–472.
Kajiwara, S., 1981. Philos. Mag. 43, 1483.
Kajiwara, S., 1984. Acta Metall. 32, 407.
Karma, A., Rappel, W.J., 1998. Phys. Rev. E 57, 4323.
Khachaturyan, A.G., 1983. Theory of Structural Transformations in Solids. J. Wiley and Sons, New York, London.
Koslowski, M., Cuitino, A.M., Ortiz, M., 2002. J. Mech. Phys. Solids 50, 2597–2635.
Kundin, J., Zimmer, J., Emmerich, H., 2010. Philos. Mag. 90 (11), 1495–1510.
Kuznetsov, V.M., Kadyrov, R.I., Rudenskii, G.E., 1998. J. Mater. Sci. Technol. 14, 320.
Ma, A., Roters, F., 2004. Acta Mater. 52, 3603.
Ortiz, M., Stainier, L., 1999. Comput. Methods Appl. Mech. Eng. 171 (3–4), 419–444.
Patterson, R.L., Wayman, C.M., 1966. Acta Metall. 14, 3437.
Roters, F., Raabe, D., Gottstein, G., 2000. Acta Mater. 48, 4181–4189.
Roters, F., Eisenlohr, P., Hantcherli, L., Tjahjanto, D.D., Bieler, T.R., Raabe, D., 2010. Acta Mater. 58, 1152–1211.
Sandvik, B.P.J., Wayman, C.M., 1983. Metall. Trans. 14A, 2455.
Sato, H., Zaefferer, S., 2009. Acta Mater. 57, 1931–1937.
Shen, C., Wang, Y., 2003. Acta Mater. 51, 2595–2610.
Shen, C., Wang, Y., 2004. Acta Mater. 52, 683–691.
Takaki, T., Tomita, Y., 2010. Int. J. Mech. Sci. 52, 320–328.
Tjahjanto, D.D., Turteltaub, S., Suiker, A.S.J., 2008. Cont. Mech. Thermodyn. 19, 399.
Turteltaub, S., Suiker, A.S.J., 2006. Int. J. Solids Struct. 43, 4509.
Umemoto, M., Tamura, I., 1982. J. Phys. Colloq. 43, 523.
Umemoto, M., Yoshitake, E., Tamura, I., 1983. J. Mater. Sci. 18, 2893.
Wang, Y., Khachaturyan, A.G., 1997. Acta Mater. 45, 759–773.
Wang, Y.U., Jin, Y.M., Cuitino, A.M., Khachaturyan, A.G., 2001. Acta Mater. 49, 1847–1857.
Wayman, C.M., 1964. Introduction to the Crystallography of Martensitic Transformation. Macmillan, New York.
Yamanaka, A., Takaki, T., Tomita, Y., Yoshino, M., 2009. Crystal plasticity phase-field simulation of deformation behavior and microstructure evolution in polycrystalline material. In: Proceedings of X International Conference on Computational Plasticity - COMPLAS X (CD-ROM), vol. 462, 2009, pp. 1–4.
Yang, D-Z., Sandvik, B.P.J., Wayman, C.M., 1984. Metall. Trans. 15A, 1555.
Zhou, N., Shen, C., Mills, M.J., Wang, Y., 2010. Philos. Mag. 90, 405–436.